Effect of Gradation on the Strength and Stress-Dilation Behavior of Coarse-Grained Soils in Drained and Undrained Triaxial Compression

Sheikh Sharif Ahmed[1]; Alejandro Martinez, A.M.ASCE[2]; and Jason T. DeJong, F.ASCE[3]

Abstract: Geotechnical engineering practice commonly estimates the properties and behavior of well-graded soils using methods and relationships developed based on the behavior of clean, poorly graded coarse-grained soils. The influence of gradation on the strength and stress-dilatancy behavior of coarse-grained soils is complex because it depends on the soil state, which is complicated by the use of parameters that can bias and obscure the effects of gradation (i.e., void ratio versus relative density or state parameter). This study examines the effect of gradation and particle size on the drained and undrained triaxial compression behavior of pluviated poorly graded and well-graded soils sourced and sieved from a single deposit. A series of 69 triaxial tests were performed on soil specimens with a range of initial state parameters. Wider gradations resulted in a reduction in the slope and intercept of the critical state line (CSL), whereas increasing particle size for poorly graded soils resulted in an increase in the CSL slope and intercept. The results indicate an increase in peak friction angle and maximum dilation angle for soils with wider gradations for any given state parameter. The peak drained and undrained strengths at any given state parameter are shown to increase with range of particle sizes as a result of the increase in dilative tendencies. However, the contribution of the maximum rate of dilatancy to the difference between the peak and critical state friction angles appears to be unaffected by gradation. Finally, the Bolton framework was found to underpredict the difference between peak and critical state friction angles at any given relative density.
DOI: 10.1061/JGGEFK.GTENG-10972.

Author keywords: Coarse-grained soils; Well-graded soils; Stress dilatancy; Triaxial compression; Mean particle size; Gradation.

Introduction

The mechanical behavior of coarse-grained soils is governed by inherent particle properties such as shape, gradation, surface roughness, and mineralogy. The strength of these soils is commonly characterized by the angle of internal friction and its dependency on dilatancy, which is a function of the combination of density (i.e., void ratio, e, or porosity, n) and the magnitude of applied effective stresses, typically referred to as the soil state. Although soil strength is a fundamental parameter for geotechnical engineering design, there is uncertainty in its estimation using both laboratory and in situ testing methods. A number of knowledge gaps and limitations with existing studies remain due to the challenges associated with sampling and testing of well-graded coarse-grained soils (e.g., Daniel et al. 2004; Goto et al. 1994; Kokusho and Tanaka 1994; Yoshimi et al. 1994; Singh et al. 1982). Particularly, the effects of gradation on the strength and stress-dilatancy behavior of coarse-grained soils are complex because they depend on the soil state. Indeed, seemingly contradictory conclusions can be obtained when using different parameters to characterize the soil state, such as the void ratio, relative density (D_R), and the difference in void ratio between a given state and the critical state [termed the state parameter, ξ, by Been and Jefferies (1985)].

Dilatancy of soils refers to the change in volume due to shear deformations (Reynolds 1885). The stress-dilatancy relationships capture the dependence of the soil strength on the dilation of coarse-grained soils. Since the early work of Taylor (1948), several stress-dilatancy frameworks have been proposed based on either theoretical (e.g., Skempton and Bishop 1950; Bishop 1954; Newland and Allely 1957; Rowe 1962, 1969; Schofield and Wroth 1968; De Josselin de Jong 1976; Yang and Li 2004) or experimental (e.g., Lee and Seed 1967; Bolton 1986; Negussey et al. 1988; Vaid and Sasitharan 1992; Chakraborty and Salgado 2010) studies. Rowe (1962) derived the saw blade stress-dilatancy model for an assembly of uncrushable particles based on the minimum energy principle, which was later validated by De Josselin de Jong (1976) with an alternative approach based on the laws of friction. Bolton (1986) derived stress-dilatancy correlations based on direct simple shear and triaxial compression test results on poorly graded sands, and proposed a relative density index (I_R) that accounted for the effects of both relative density and confining effective stress. Further stress-dilatancy relations clearly demonstrated the effects of particle shape, stress history, density, fabric, and confining effective stress (e.g., Vermeer and de Borst 1984; Pradhan et al. 1989; Houlsby 1991; Gudehus 1996; Nakai 1997; Wan and Guo 1998, 1999; Vaid and Saivathayalan 2000; Guo and Su 2007; Yang and Luo 2015). Given that existing stress-dilatancy relations and the current general understanding of soil dilative tendencies were largely developed based on experiments on poorly graded sands, further investigation is needed to assess their applicability to well-graded materials.

[1]Operations Manager, Center for Geotechnical Modeling, Univ. of California, 655 Brooks Rd., Davis, CA 95616. Email: ssah@ucdavis.edu

[2]Associate Professor, Dept. of Civil and Environmental Engineering, Univ. of California, 2001 Ghausi Hall, Davis, CA 95616 (corresponding author). ORCID: https://orcid.org/0000-0003-4649-925X. Email: amart@ucdavis.edu

[3]Professor, Dept. of Civil and Environmental Engineering, Univ. of California, 2001 Ghausi Hall, Davis, CA 95616. ORCID: https://orcid.org/0000-0002-9809-955X. Email: jdejong@ucdavis.edu

Note. This manuscript was submitted on April 14, 2022; approved on January 4, 2023; published online on February 22, 2023. Discussion period open until July 22, 2023; separate discussions must be submitted for individual papers. This paper is part of the ***Journal of Geotechnical and Geoenvironmental Engineering***, © ASCE, ISSN 1090-0241.

In recent years, researchers have investigated the effects of gradation and particle size on the strength and stress-dilatancy of coarse-grained soils. Consistent trends can be summarized as follows:

- Generally, as gradation becomes broader (i.e., the coefficient of uniformity, C_u, increases), the maximum and minimum void ratios (e_{max} and e_{min}, respectively) decrease, and the location of the critical state line (CSL) in e versus mean effective stress (p') space (i.e., e- log p' space) shifts downward (e.g., Youd 1973; Li et al. 2015; Liu et al. 2014; Wood and Maeda 2008).
- The slope of the CSL decreases with increasing C_u for coarse-grained soils due to the increase in stiffness, but the soil may become more compressible if plastic fines are present (e.g., Li et al. 2015; Been and Jefferies 1985).
- For the same initial void ratio, more widely graded soils tend to exhibit a greater contractive behavior, lower undrained strengths, and higher susceptibility to liquefaction due to their increased distance from the CSL (i.e., increasing state parameter) (e.g., Liu et al. 2014; Li et al. 2015; Yan and Dong 2011).
- In the absence of differences in particle shape, gradation and particle size exhibit no systematic or significant effect on the critical state friction angle (e.g., Yang and Luo 2017; Jiang et al. 2018; Voivret et al. 2009; Harehdasht et al. 2017, 2018; Deng et al. 2021).
- The small-strain stiffness generally increases with increasing coefficient of uniformity (e.g., Chang and Ko 1982; Kokusho and Yoshida 1997; Menq 2003; Sturm 2019).
- Changes in the strength and index properties appear to saturate as C_u approaches about 30 (e.g., Liu et al. 2014).
- The behavior of soils with increasing gravels content (or broader gradation) is typically controlled by the interactions of the coarser particles as well as the decreased void ratio (e.g., Fragaszy et al. 1990, 1992; Evans and Zhou 1995).
- Increasing gradation results in an increase in contact numbers (i.e., coordination number) for the coarser particles of the assembly (e.g., Yi et al. 2011; Liu et al. 2021).

Despite the aforementioned insights, many of the previously published studies have been performed on the basis of a fixed void ratio or have been concerned mainly with the critical state behavior. Because the CSL location and the maximum and minimum void ratios are affected by the gradation, adopting the void ratio as a reference state parameter when evaluating behaviors that depend on the volumetric response of the soil (i.e., mobilization of peak strengths and generation of excess pore pressures) can bias the interpretation and conclusions of a given study. Alternatively, a state parameter that accounts for the effects of gradation on the range of attainable void ratios may be more appropriate. Namely, the use of D_R or ξ may provide a more robust basis for interpretation of the effects of gradation on the stress-dilatancy behavior of coarse-grained soils.

This study aims to systematically examine the role of D_{50} and C_u on the stress-dilatancy behavior of well-graded coarse-grained soils by means of triaxial compression tests. A well-graded natural sand was selectively sieved to produce different sands with similar particle-shape parameters but with different gradation and D_{50}. A series of isotropically consolidated drained (ICD) and undrained (ICU) triaxial tests were performed on specimens with a range of initial D_R and confining effective stresses to define their CSLs, and the results were interpreted based on the ξ corresponding to each specimen. The applicability of using poorly graded sand-based methods with well-graded coarse-grained soils is evaluated through Bolton (1986)'s empirical framework.

Materials and Methods

Soils of Varying Gradation and Particle Size

Six coarse-grained soils with different particle sizes and gradations were used in thi study (Fig. 1). All the soils were composed of quartz sand and gravel-sized particles sourced from the Cape May Formation near Mauricetown, New Jersey. The source soil was mechanically sieved into seven poorly graded portions (100A, 100B, 100C, 100D, 100E, 100–140, and 140–200), ranging in median particle size, D_{50}, from 0.13 to 4.20 mm (Pires-Sturm and DeJong 2022). Three of these portions (100A, 100C, and 100D) were selected for testing to capture the effect of D_{50} on the behavior of poorly graded soil while minimizing variability regarding mineralogy, particle shape, and gradation.

To compare the behavior of these poorly graded soils with that of well-graded soils, three well-graded sand-gravel mixtures (33ABC, 25ABCD, and 12CU) were formed from the poorly graded soil portions: 33ABC contains equal mass proportions of 100A, 100B, and 100C; 25ABCD contained equal mass proportions of 100A, 100B, 100C, and 100D; and 12CU contained all

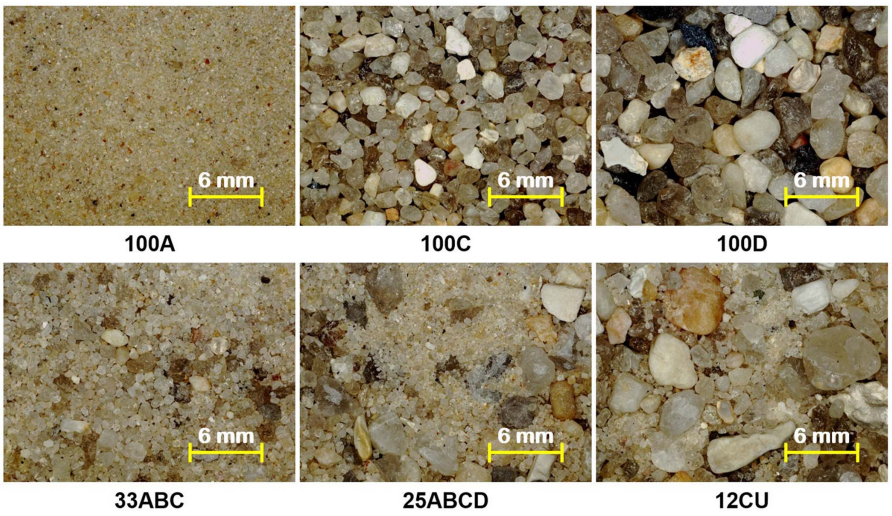

Fig. 1. Soils used in this study.

J. Geotech. Geoenviron. Eng., 2023, 149(5): 04023019

Table 1. Properties of the soils used in this study

Soil	D_{10} (mm)	D_{30} (mm)	D_{50} (mm)	D_{60} (mm)	C_u	C_c	e_{max}	e_{min}	Roundness	Sphericity	G_s
100A	0.12	0.16	0.18	0.20	1.74	1.04	0.881	0.579	0.39 (0.11)	0.74 (0.13)	2.62
100C	0.91	1.13	1.31	1.39	1.53	1.01	0.839	0.557	0.42 (0.12)	0.75 (0.12)	2.61
100D	1.79	2.21	2.58	2.74	1.53	1.00	0.812	0.540	0.45 (0.09)	0.75 (0.12)	2.60
33ABC	0.15	0.26	0.51	0.66	4.40	0.68	0.622	0.397	0.40 (0.11)	0.75 (0.12)	2.61
25ABCD	0.23	0.53	0.80	1.71	7.43	0.71	0.544	0.303	0.41 (0.12)	0.75 (0.12)	2.61
12CU	0.18	0.66	1.55	2.20	12.34	1.11	0.450	0.276	0.46 (0.12)	0.75 (0.12)	2.61

Note: The values in parenthesis represent standard deviation.

seven poorly graded soil portions in different mass proportions (5% 100–140, 140–200, and 100A; 19% 100B and 100C; and 24% 100D and 100E). These six soils capture a range in the C_u values from 1.53 to 12.34. Table 1 presents a summary of the physical and index properties of the soils tested, and Fig. 2(a) shows the grain-size distributions.

The maximum (e_{max}) and minimum (e_{min}) void ratios of the test soils were determined by the method of Sturm (2019) following Method A of ASTM D4254-16 (ASTM 2016b) and Method 1B of ASTM D4253-16 (ASTM 2016a), respectively. As shown in Fig. 2(b), the poorly graded soils (100A, 100C, and 100D) have similar e_{max} (0.812–0.881) and e_{min} (0.540–0.579) values, and both e_{max} and e_{min} significantly decreased with increasing C_u. These trends are consistent with those previously reported in literature (e.g., Youd 1973). The roundness and sphericity of the six tested soils was determined using the method and MATLAB version 9.4 code proposed by Zheng and Hryciw (2015). The tested soils all had similar particle shape parameters, with roundness in the range of 0.39–0.46 and sphericity in the range of 0.74–0.75. Based on the similar particle shape parameters, the differences in soil behavior observed throughout this investigation are attributed to the effects of gradation and particle size.

Triaxial Test

Monotonic drained and undrained isotropically consolidated triaxial compression tests were performed to characterize the response of specimens of all six soils. An automatic triaxial testing system with digital data acquisition capabilities, developed by GeoTac (Houston, Texas), was used in testing. Cell and pore pressures and volume change were controlled using two digital pressure volume controllers. The measured volume changes were used to determine the specimen volumetric strain, ε_v. The applied axial load was measured by an external load cell mounted onto the load frame, and the axial displacement was measured by an external linear variable differential transducer, which was used to determine the specimen axial strain, ε_a. All the load and displacement results were corrected for piston friction and machine compliance. Pore pressure transducers were used to measure the specimen pore pressure as well as the triaxial confining pressure.

Tests were performed on specimens of 70-mm diameter and 150-mm height. This size gives a specimen diameter-to-D_{50} ratio of 27 for 100D specimens and a specimen diameter-to-D_{max} ratio of 5.8 for 12CU specimens. Pluviation of dry particles from a constant height was used to prepare specimens; this sample preparation technique was employed in order to maximize density and fabric uniformity (e.g., Miura and Toki 1982; Vaid and Negussey 1984; Vaid et al. 1999; Lagioia et al. 2006) and is the same as that used in studies on the same materials by Sturm (2019) and Humire (2022). Sturm (2019), Sawyer (2020), Humire (2022), and Carey et al. (2022) assessed the uniformity of 100A, 100C, 100D, 33ABC, 25ABCD, and 12CU specimen prepared using the same dry pluviation technique, concluding that dry pluviation produces homogenous specimens. This was checked during the current testing campaign by visual inspection.

Specimens were prepared at target loose ($D_R = 15\%–30\%$), medium-dense ($D_R = 40\%$), and dense ($D_R = 65\%–90\%$) states. Each prepared specimen was stabilized by an applied vacuum of 10 kPa, then placed in the triaxial cell and the cell was filled with deaired water. The specimen was flushed with CO_2 and then saturated by applying back-pressure while maintaining a constant difference of 30 kPa between the cell pressure and back-pressure. Afterward, the back-pressure was increased slowly until a B-value of 0.95 or greater was achieved. Although the axial LVDT indicated

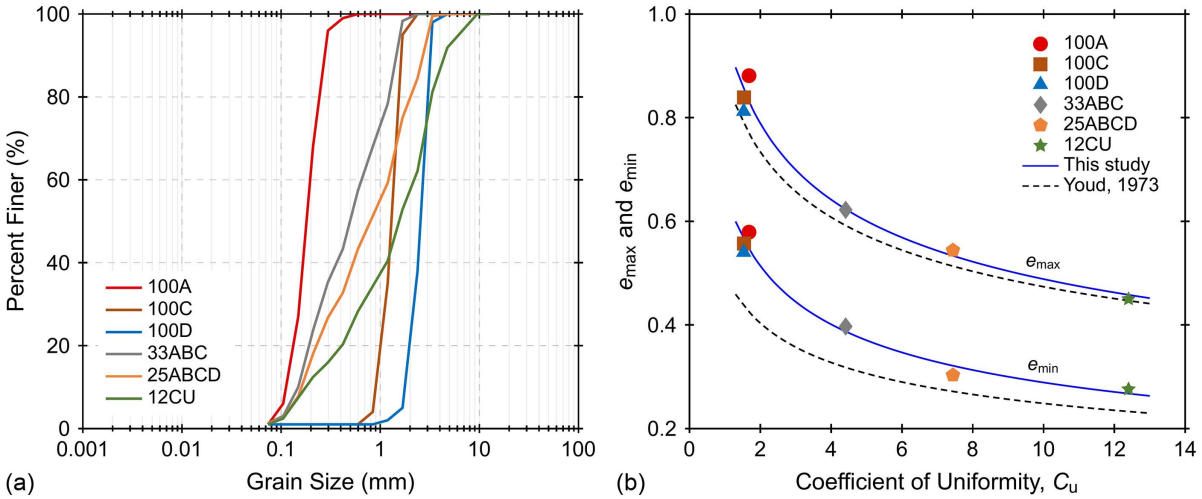

Fig. 2. (a) Gradation of the soils used in this study; and (b) variation of maximum and minimum void ratios with coefficient of uniformity.

no change in the specimen height during the flushing and saturation process, the diameter may have decreased due to contraction during wetting, particularly for the specimens at very loose states. After saturation, the specimen was consolidated isotropically to the target confining pressure. Once the consolidation phase to the target confining pressure was completed, the shearing phase commenced at a strain rate of 10%/h. Cavitation during undrained tests was not observed in any of the experiments. Appropriate membrane penetration correction for the volume changes was applied to the specimens of 100D and 12CU (Kramer et al. 1990); the membrane penetration correction was found to be insignificant for the 100A, 100C, 33ABC, and 25ABCD soils.

In total, 33 drained and 36 undrained triaxial tests were performed at effective stresses (σ'_{3c}) ranging from 50 to 500 kPa, as indicated in Tables 2 and 3, respectively. It was not expected that significant particle crushing took place at these stress levels, which was confirmed by visual inspection of the posttest soils. The testing ID convention is such that ID P-x-Q-y corresponds to soil P at x% relative density tested at Q condition (CD = consolidated drained, CU = consolidated undrained) at a σ'_{3c} of y kPa. For example, 100A-65-CD-500 corresponds to soil 100A at 65% relative density tested at drained condition at σ'_{3c} of 500 kPa.

Results

A total of 69 triaxial compression tests were performed on soils of varying gradation and particle size but with similar particle shapes. This section first describes the drained and undrained response of specimens of different initial D_R subjected to different magnitudes of σ'_{3c}. Then, the results are used to estimate CSLs for the soils. Finally, the trends in parameters that describe the specimens' response such as peak and critical state friction angles, maximum dilation angles, and pore pressure generation magnitudes and rates are interpreted on the basis of the initial state parameter of the specimens.

Triaxial Compression Behavior

Triaxial tests revealed that the gradation influenced the strength and volume-change behavior of the soils. This section presents the results in terms of deviatoric stress (q)-axial strain (ε_a), volumetric strain (ε_v)-axial strain (ε_a), excess pore pressure (Δu)-ε_a, q–mean effective stress (p'), and e- log p' curves for tests performed on 100A, 100D, and 25ABCD soils. The corresponding results from tests on 100C, 33ABC, and 12CU soils are included as Figs. S1–S4.

Isotropic Compression Response

Fig. 3 shows the isotropic compression response for all the sands with different initial relative densities and confining pressures. Of the poorly graded soils (i.e., 100A, 100C, 100D), those with greater median particle size had a greater decrease in void ratio with increasing mean effective stress [Figs. 3(a–c)]. The decrease in void ratio with increasing mean effective stress slightly increased as gradation became broader for the broadly graded soils [Figs. 3(d–f)].

The variation of the average slopes of the compression curves (i.e., compressibility index, C_c) with C_u and D_{50} for all the soils are shown in Figs. 4(a and b), respectively. The C_c values increased as both C_u and D_{50} increased. However, the variations in D_{50} appear to better-capture the changes in C_c, as shown in Fig. 4(b). This can be explain by the fact that the force carried by a particle increases at a faster rate with particle size than its stiffness. Indeed, Hertz theory states theory states that the interparticle contact stiffness increases with particle radius to the 1/3 power while the force carried by a contact increases with radius to the 2 power (Santamarina et al. 2001)

Drained Shearing Response

The drained deviatoric stress and volumetric change responses for the 100A, 100D, and 25ABCD soils with different initial target relative densities (i.e., 15%–30%, 40%, and 65%) at the same cell pressure ($\sigma'_{3c} = 100$ kPa) are shown in Fig. 5. As expected, greater peak deviatoric stresses and stiffer initial responses were exhibited by the specimens with higher initial relative density for all three soils [Figs. 5(a, e, and i)]. The q-ε_a curves for all the dense ($D_R \approx 65\%$) specimens exhibited a distinct peak followed by strain softening [Figs. 5(a, e, and i)], and were accompanied by large dilative volumetric strains [Figs. 5(b, f, and j)], where dilation is defined as negative and contraction as positive. The q-ε_a curves for all the medium dense ($D_R \approx 40\%$) specimens exhibited a slight peak deviatoric stress, followed by strain softening and were accompanied by dilative volumetric strains. Finally, the q-ε_a curves for all the loose ($D_R \approx 15$–30%) specimens showed strain hardening accompanied by initial volumetric contraction, followed by slight dilation at axial strains greater than about 3%.

As shown, for the dense and medium-dense specimens, the peak in the q-ε_a curves was more pronounced for the 25ABCD soil than for the 100A and 100D soils. The tests on 100C, 33ABC, and 12CU soils showed the same trends (Figs. S1 and S2). The curves in the q-p' plane followed the expected stress paths for drained triaxial compression [Figs. 5(c, g, and k)], whereas the stress paths in the e- log p' plane showed a greater amount of dilation exhibited by the tests with greater initial D_R [Figs. 5(d, h, and l)]. These stress paths also clearly showed the smaller e values attained by the well-graded 25ABCD soil. All the 100A and 100D specimens exhibited a barreling failure without clear shear bands. However, the 25ABCD-65-CD-100 specimen exhibited a shear band that may have been responsible for the large strain softening observed at ε_a between 3% and 7% [Fig. 5(i)] and the sharp reduction in incremental dilative strains at greater ε_a values [Fig. 5(j)].

Fig. 6 shows drained triaxial compression results of loose specimens sheared at different σ'_{3c}. As expected, greater deviatoric stresses were mobilized by the specimens at higher σ'_{3c} [Figs. 6(a, e, and i)]. The q-ε_a curves for all the sand specimens exhibited strain hardening under all σ'_{3c} considered. The volumetric strain response exhibited a dependency on σ'_{3c}, with greater contractive volumetric strains for specimens at greater σ'_{3c} for all three soils, and all the specimens exhibited overall contractive volumetric strains at σ'_{3c} of 500 kPa [Figs. 6(b, f, and j)]. The stress paths in the e- log p' plane clearly showed the initial contraction observed in the tests performed at σ'_{3c} of 100 and 200 kPa as well as the overall contractive response of the tests performed at σ'_{3c} of 500 kPa [Figs. 6(d, h, and l)].

Undrained Shearing Response

Fig. 7 shows the deviatoric stress and excess pore pressure change responses during undrained shearing for soils 100A, 100D, and 25ABCD with different initial relative densities at a σ'_{3c} of 100 kPa. The dense ($D_R \approx 65\%$) specimens of all the soils mobilized the greatest deviatoric stresses, whereas the loose ($D_R = 15\%$–30%) specimens mobilized the smallest deviatoric stresses [Figs. 7(a, e, and i)]. These trends in strength are a result of the negative excess pore pressures (Δu) generated by the dense specimens and the positive or slightly negative Δu generated by the loose specimens.

In agreement with the drained test results shown in Figs. 5(a–l), the response of the dense specimens was dilative whereas that of

Table 2. List of drained triaxial tests

Soil	Test ID	Confining pressure, σ'_{3c} (kPa)	Void ratio at end of consolidation, e_{eoc}	Relative density at end of consolidation, $D_{R(eoc)}$ (%)	State parameter at end of consolidation, ξ	Critical state			Peak deviatoric stress			
						Mean effective stress, p'_{cs} (kPa)	Deviatoric stress, q_{cs} (kPa)	Void ratio, e_{cs}	Mean effective stress, p'_{peak} (kPa)	Deviatoric stress, q_{peak} (kPa)	Peak friction angle, φ'_{peak} (degrees)	Maximum dilation angle, ψ'_{max} (degrees)
100A	100A-LOOSE-CD-100	100	0.812	23	−0.04	178	235	0.844	194	281	35.9	4.7
	100A-LOOSE-CD-200	200	0.806	25	−0.03	353	460	0.816	369	509	34.2	3.1
	100A-LOOSE-CD-500	500	0.788	31	−0.02	867	1,100	0.781	895	1,185	33.0	3.2
	100A-40-CD-100	100	0.757	41	−0.10	—	—	—	202	305	37.2	7.9
	100A-65-CD-100	100	0.684	65	−0.17	—	—	—	229	390	41.7	17.5
100C	100C-LOOSE-CD-100	100	0.800	14	−0.10	187	260	0.845	198	293	36.7	5.7
	100C-LOOSE-CD-200	200	0.771	24	−0.08	360	480	0.796	376	529	34.8	4.6
	100C-LOOSE-CD-500	500	0.764	27	−0.02	867	1,100	0.738	868	1,103	31.6	0.0
	100C-LOOSE-CD-700	700	0.753	30	−0.01	1,209	1,526	0.709	1,210	1,528	31.4	0.0
	100C-40-CD-100	100	0.729	39	−0.17	—	—	—	209	322	38.0	9.4
	100C-65-CD-100	100	0.655	65	−0.24	—	—	—	239	410	41.8	18.9
100D	100D-LOOSE-CD-100	100	0.766	17	−0.09	187	262	0.802	195	286	36.1	5.6
	100D-LOOSE-CD-200	200	0.751	23	−0.04	359	476	0.742	366	496	33.8	1.6
	100D-LOOSE-CD-500	500	0.720	34	0.00	887	1,160	0.659	860	1,079	31.4	0.0
	100D-40-CD-100	100	0.693	44	−0.16	—	—	—	216	350	39.7	11.9
	100D-65-CD-100	100	0.623	69	−0.23	—	—	—	243	428	43.1	19.8
33ABC	33ABC-LOOSE-CD-100	100	0.572	22	−0.04	187	262	0.591	195	286	36.1	3.6
	33ABC-LOOSE-CD-200	200	0.562	27	−0.03	367	502	0.572	379	536	35.0	2.5
	33ABC-LOOSE-CD-500	500	0.574	21	0.00	900	1,200	0.551	901	1,201	33.0	0.9
	33ABC-LOOSE-CD-700	700	0.572	22	0.01	1,255	1,666	0.539	1,256	1,671	33.0	0.6
	33ABC-40-CD-100	100	0.530	41	−0.09	—	—	—	208	324	38.5	8.1
	33ABC-65-CD-100	100	0.476	65	−0.14	—	—	—	232	399	42.0	15.6
25ABCD	25ABCD-LOOSE-CD-100	100	0.506	16	−0.03	188	265	0.516	196	288	36.3	3.2
	25ABCD-LOOSE-CD-200	200	0.506	16	−0.01	371	512	0.510	383	550	35.6	2.4
	25ABCD-LOOSE-CD-500	500	0.498	19	0.00	918	1,255	0.479	924	1,257	33.8	0.6
	25ABCD-40-CD-100	100	0.449	39	−0.08	—	—	—	217	351	39.5	11.1
	25ABCD-65-CD-100	100	0.387	65	−0.15	—	—	—	252	455	44.0	20.8
12CU	12CU-LOOSE-CD-100	100	0.420	17	−0.03	193	280	0.428	203	308	37.4	3.3
	12CU-LOOSE-CD-200	200	0.413	21	−0.02	375	526	0.418	381	545	35.4	1.6
	12CU-LOOSE-CD-500	500	0.409	24	−0.01	947	1,340	0.401	951	1,353	35.2	1.0
	12CU-40-CD-100	100	0.373	44	−0.07	—	—	—	210	330	38.7	10.7
	12CU-65-CD-100	100	0.334	66	−0.11	—	—	—	233	399	42.0	14.4
	12CU-90-CD-100	100	0.293	90	−0.15	—	—	—	272	512	46.4	22.5

Table 3. Details of the undrained tests

Soil	Test ID	Confining pressure, σ'_{3c} (kPa)	Void ratio at end of consolidation, e_{eoc}	Relative density at end of consolidation, $D_{R(eoc)}$ (%)	State parameter at end of consolidation, ξ	Critical state			Peak		Minimum excess pore pressure, Δu_{min} (kPa)	Minimum rate of change of pore pressure, $(\delta u/d\varepsilon_a)_{min}$ (kPa)
						Mean effective stress, p'_{cs} (kPa)	Deviatoric stress, q_{cs} (kPa)	Void ratio, e_{cs}	Mean effective stress, p'_{peak} (kPa)	Deviatoric stress, q_{peak} (kPa)		
100A	100A-LOOSE-CU-50	50	0.811	23	−0.07	237	306	0.811	228	306	−72	−9
	100A-LOOSE-CU-100	100	0.819	21	−0.04	383	504	0.819	384	504	−112	−11
	100A-LOOSE-CU-200	200	0.815	22	−0.02	361	472	0.815	361	473	0	−12
	100A-LOOSE-CU-500	500	0.795	28	−0.01	655	853	0.795	655	854	0	−19
	100A-40-CU-100	100	0.754	42	−0.10	—	—	—	745	996	−315	−31
	100A-65-CU-100	100	0.688	64	−0.17	—	—	—	968	1,408	−414	−77
100C	100C-LOOSE-CU-50	50	0.793	16	−0.15	445	607	0.793	445	610	−195	−16
	100C-LOOSE-CU-100	100	0.787	18	−0.11	522	699	0.787	523	702	−200	−18
	100C-LOOSE-CU-200	200	0.776	22	−0.07	595	779	0.776	597	782	−136	−20
	100C-LOOSE-CU-500	500	0.757	29	−0.03	753	982	0.757	759	984	0	−18
	100C-40-CU-100	100	0.729	39	−0.17	—	—	—	709	950	−295	−35
	100C-65-CU-100	100	0.654	66	−0.24	—	—	—	856	1,261	−344	−70
100D	100D-LOOSE-CU-50	50	0.777	13	−0.14	240	327	0.777	240	329	−77	−10
	100D-LOOSE-CU-100	100	0.767	17	−0.09	253	335	0.767	255	350	−41	−11
	100D-LOOSE-CU-200	200	0.757	20	−0.04	345	455	0.757	350	463	0	−10
	100D-LOOSE-CU-500	500	0.724	32	0.01	525	688	0.724	544	723	0	−8
	100D-40-CU-100	100	0.692	44	−0.16	—	—	—	581	790	−219	−28
	100D-65-CU-100	100	0.630	67	−0.22	—	—	—	738	1,069	−290	−47
33ABC	33ABC-LOOSE-CU-50	50	0.602	9	−0.03	163	235	0.602	163	237	−39	−6
	33ABC-LOOSE-CU-100	100	0.597	11	−0.02	200	279	0.597	201	281	−9	−5
	33ABC-LOOSE-CU-200	200	0.585	17	−0.01	292	393	0.585	292	396	0	−6
	33ABC-LOOSE-CU-500	500	0.567	25	0.00	506	666	0.567	517	672	0	−9
	33ABC-40-CU-100	100	0.530	41	−0.09	—	—	—	519	745	−169	−33
	33ABC-65-CU-100	100	0.473	66	−0.14	—	—	—	800	1,137	−321	−61
25ABCD	25ABCD-LOOSE-CU-50	50	0.515	12	−0.03	189	263	0.515	189	264	−49	−8
	25ABCD-LOOSE-CU-100	100	0.506	16	−0.03	331	458	0.506	332	458	−80	−12
	25ABCD-LOOSE-CU-200	200	0.502	17	−0.02	425	576	0.502	425	578	−27	−13
	25ABCD-LOOSE-CU-500	500	0.497	20	0.00	593	795	0.497	593	796	0	−8
	25ABCD-40-CU-100	100	0.442	42	−0.09	—	—	—	790	1,105	−313	−50
	25ABCD-65-CU-100	100	0.389	64	−0.14	—	—	—	997	1,530	−407	−83
12CU	12CU-LOOSE-CU-50	50	0.432	11	−0.03	210	309	0.432	210	310	−57	−40
	12CU-LOOSE-CU-100	100	0.428	12	−0.02	335	472	0.428	336	475	−73	−13
	12CU-LOOSE-CU-200	200	0.420	17	−0.01	391	543	0.420	393	545	−14	−12
	12CU-LOOSE-CU-500	500	0.407	25	−0.01	641	885	0.407	643	899	0	−7
	12CU-40-CU-100	100	0.374	44	−0.07	—	—	—	637	916	−224	−34
	12CU-65-CU-100	100	0.335	66	−0.11	—	—	—	808	1,218	−304	−45

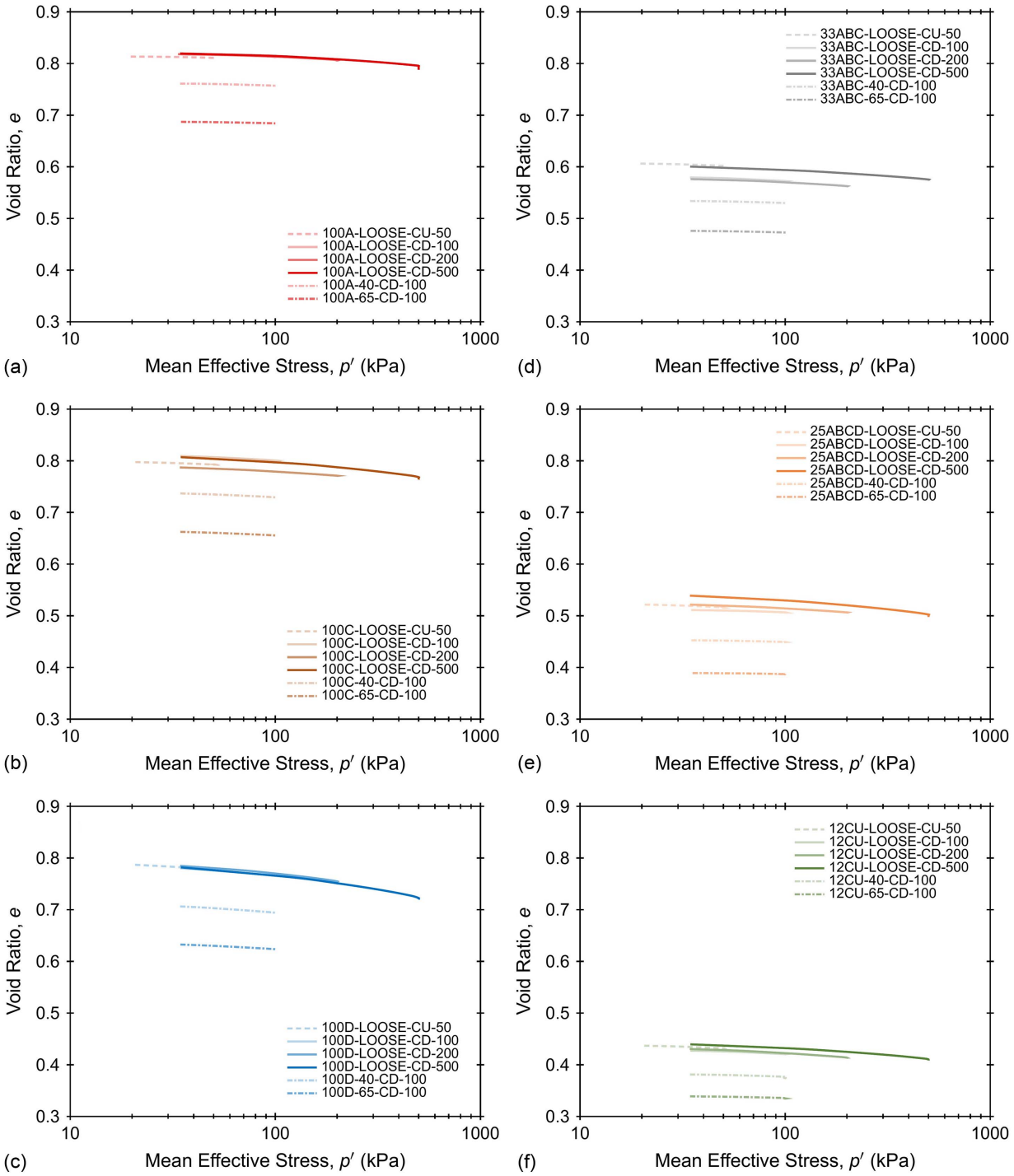

Fig. 3. Isotropic compression curves for specimens of (a) 100A; (b) 100C; (c) 100D; (d) 33ABC; (e) 25ABCD; and (f) 12CU.

the loose specimens was slightly contractive. The differences in the response can be seen in the stress paths in q-p' space, showing an initial decrease in p' for the loose tests [Figs. 7(c, g, and k)]. Additionally, the magnitudes of generated excess pore pressures were generally smaller for 100D soil than for 100A and 25ABCD. The tests on 100C, 33ABC, and 12CU soils showed the same trends (Figs. S3 and S4)

Fig. 8 shows the results of undrained tests performed on loose specimens at different σ'_{3c}. Specimens under the highest σ'_{3c} mobilized the greatest deviatoric stress [Figs. 8(a, e, and i)], as well as the greatest positive excess pore pressures [Figs. 8(b, f, and j)]. These trends agree with the greater contractive behavior observed at larger cell pressures in the drained tests (Fig. 6). The excess pore pressures in the undrained tests reached a maximum positive value and then decreased to a lower positive value, indicating overall contractive volumetric response. All the specimens under σ'_{3c} of 100 kPa generated small positive Δu, which reduced to negative Δu values, indicating small initial volumetric contraction followed by dilative response. On the other hand, all the specimens under σ'_{3c} of 500 kPa generated positive Δu. The stress paths in q-p' space show that the 100A specimens exhibited a greater initial decrease in mean effective stress; however,

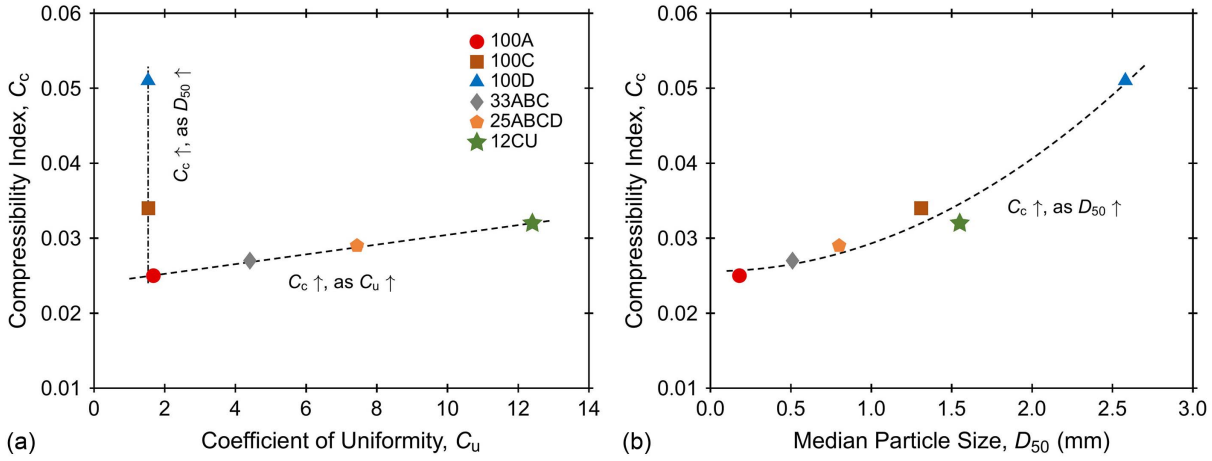

Fig. 4. Variation of compressibility index C_c with (a) C_u; and (b) D_{50}.

all three soils mobilized similar q values at the end of the tests [Figs. 8(c, g, and k)].

Critical State Lines and the Effect of Gradation and Particle Size

The points at the end of shearing for the loose specimens of all six soils (Figs. 6 and 8) were considered to have reached the critical state, which were used to estimate the CSLs in the q-p' plane. As shown in Fig. 9, the critical state points obtained from the tests on loose specimens can be fitted with a straight line passing through the origin with a slope M that can be used to obtain the critical state friction angle, ϕ'_{cs}. The critical state points in e- log p' space for all the soils were approximated from both drained and undrained tests on loose specimens. These points were obtained for CD and CU tests by extrapolating the end-of-test results following the methods described by Zhang et al. (2018) and Torres-Cruz and Santamarina (2020), respectively. Examples of the extrapolation procedures are presented in Fig. S5, which consist of extrapolating the dilatancy to a value of 1.0 in drained tests and the rate of pore pressure change to a value of zero in undrained tests. The extrapolated points in the e- log p' plane for all the soils are shown in Fig. 10. The critical state line was defined using the following logarithmic function:

$$e_{cs} = e_\Gamma - \lambda \log p' \tag{1}$$

where e_{cs} = critical state void ratio at a given p'; e_Γ = critical state void ratio at $p' = 1$ kPa; and λ = critical state line slope. Fig. 10 shows the critical state line equations for all the soils. CSLs in the e- log p' plane could also be approximated using a power function, which would appear curved in semilog space, as presented by Wang et al. (2002). However, due to the lack of clear curvature in the range of p' values considered in this study, a linear approximation was chosen for the interpretation.

The CSL parameters M (i.e., slope in q -p' space or critical state ratio), e_Γ, and λ appear to be influenced by the soil gradation and particle size; the effect of these parameters is discussed in terms of C_u and D_{50}. All three poorly graded soils (i.e., 100A, 100C, and 100D) had similar M-values between 1.29 and 1.32 ($\phi'_{cs} = 32.1°$ and 32.8°) [Figs. 11(a and d)] [i.e., $\sin(\phi'_{cs}) = 3M/(6+M)$]. The soils with wider gradations showed a slight increase in M, with values of 1.33 ($\phi'_{cs} = 33.0°$), 1.36 ($\phi'_{cs} = 33.7°$), and 1.41 ($\phi'_{cs} = 34.8°$) for soils 33ABC ($C_u = 4.40$), 25ABCD ($C_u = 7.43$), and 12CU ($C_u = 12.34$), respectively. Other studies have reported either a negligible or small influence of gradation on M or ϕ'_{cs} (e.g., Yang and Luo 2017; Jiang et al. 2018; Voivret et al. 2009; Harehdasht et al. 2017, 2018), which are in general agreement with the results presented here.

The e_Γ parameter increased modestly with increasing particle size [Figs. 11(b and e)]; however, it decreased sharply as the soil gradation becomes broader. The effect of gradation on e_Γ is explained by the decrease in e_{max} and e_{min} with increasing C_u, and is in agreement with previously published results (e.g., Li et al. 2015; Liu et al. 2014; Wood and Maeda 2008). The λ parameter is shown to increase with increasing particle size, suggesting an increase in compressibility [Figs. 11(c and f)]. The λ parameter decreases as the C_u is increased [Fig. 9(f)], which is in general agreement with previously published results indicating an increase in shear stiffness for soils with a wider gradation (e.g., Altuhafi and Coop 2011; Sturm 2019; Zheng et al. 2017).

Interpretation of Trends in Terms of the State Parameter

The state parameter proposed by Been and Jefferies (1985) offers the advantage of combining the influence of confining pressure and void ratio, similar to Bolton (1986)'s corrected relative density (I_R). The steady-state line (SSL) is defined as the locus of all steady state points in the compression plane at which the soil deforms under constant effective stress and volume (i.e., void ratio). In this study, no distinction between the CSL and SSL was made, and ξ was computed as the difference between the void ratio at the end of consolidation (e_{eoc}) and the critical state void ratio (e_{cs}) based on the fitted CSLs shown in Fig. 10. This section discusses the effects of soil gradation and particle size in terms of ξ; the Supplemental Materials present the results in terms of D_R for comparison.

Drained Response

The effect of initial state on the drained behavior of all the soils was examined by plotting test results for specimens within narrow ranges of ξ. Namely, results for 100A, 33ABC, 25ABCD, and 12CU specimens at a σ'_{3c} of 100 kPa are presented in Figs. 12(a–d) for a loose state ($\xi = -0.03 \pm 0.01$), and results for all six soils at a σ'_{3c} of 100 kPa are shown in Figs. 12(e–h) for a dense state ($\xi = -0.16 \pm 0.02$). Relevant data for these experiments are provided in Table 2.

As shown by the q-ε_a curves, all the loose specimens exhibited strain-hardening behavior accompanied by initial contractive volumteric strain response, followed by slight dilative behavior.

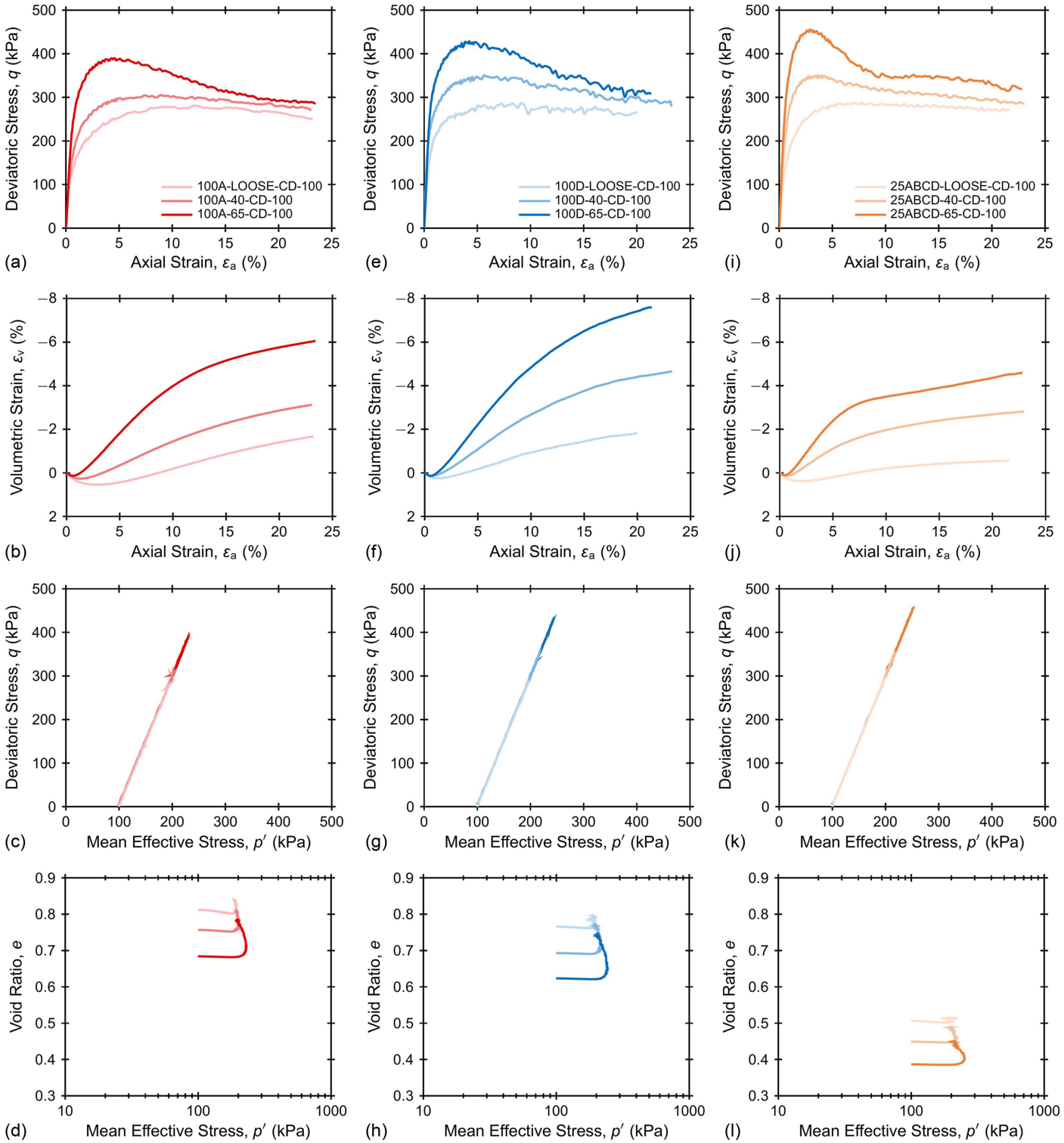

Fig. 5. ICD test results for specimens of (a–d) 100A; (e–h) 100D; and (i–l) 25ABCD at different D_R and $\sigma'_{3c} = 100$ kPa.

The 12CU specimen mobilized the greatest deviatoric stress, followed by the 25ABCD, 33ABC, and 100A specimens. The volumetic response was somewhat similar between all the soils, with the 100A specimen dilating more by the end of the test.

The dense specimens of 100A, 33ABC, 25ABCD, and 12CU exhibited a distinct peak in q followed by significant strain softening [Fig. 12(e)], whereas the 100C and 100D specimens showed only a slight peak. The greatest peak in q was mobilized by the 12CU specimen, followed by the 25ABCD, 33ABC, and 100A specimens, respectively. All specimens exhibited dilative volumetric strains, with the 12CU and 25ABCD exhibiting a greater rate of dilation at ε_a smaller than 5%, the 100C and 100D exhibiting the smallest rate of dilation, and the 100A specimen exhibiting the greatest volumetric strains by the end of the test [Fig. 10(f)].

The stress paths for the loose specimens showed similar q and p' values mobilized by all soils [Figs. 12(c and d)]. However, the stress paths for the dense specimens showed the greater q and p' values mobilized by the specimens with wider gradation [Figs. 12(g and h)].

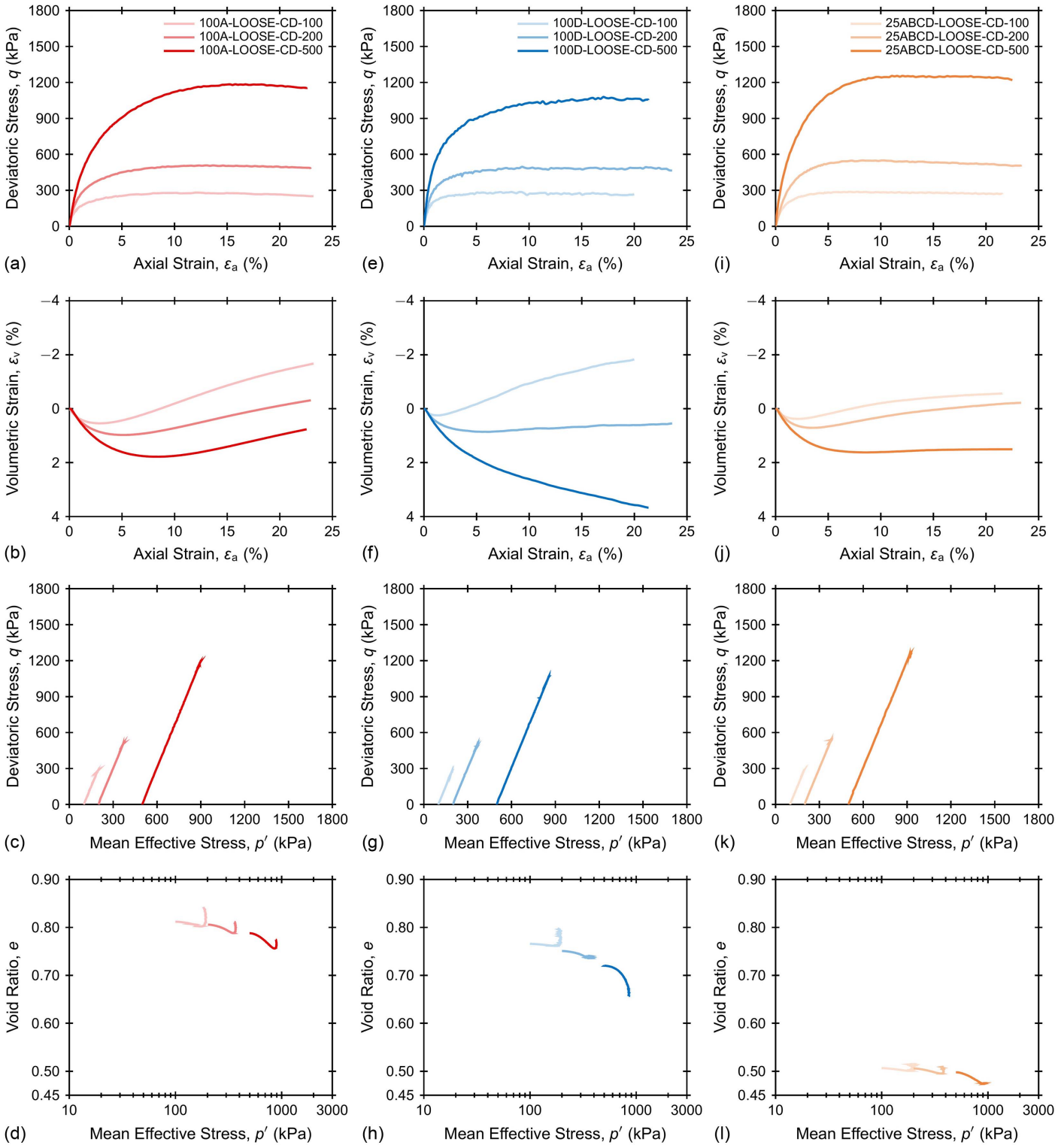

Fig. 6. ICD test results for loose specimens of (a–d) 100A; (e–h) 100D; and (i–l) 25ABCD at different σ'_{3c}.

The stress paths of both loose and dense soils showed the smaller void ratios of the specimens with wider gradations, with values between 0.29 and 0.37 for the 12CU specimen and values between 0.68 and 0.70 for the 100A, 100C, and 100D soils.

Undrained Response

The effects of initial state on the undrained behavior of all the soils were examined by plotting the undrained test results of specimens at a loose state ($\xi = -0.03 \pm 0.01$) and dense state ($\xi = -0.16 \pm 0.02$). Figs. 13(a–d) show the undrained test results of loose 100A, 33ABC, 25ABCD, and 12CU specimens, and Table 3 provides relevant data for these experiments. As shown by the q-ε_a curves, all the specimens exhibited strain-hardening behavior, and the specimens of 100A, 25ABCD, and 12CU mobilized greater deviatoric stresses compared with that of 33ABC. At smaller strains, the 12CU and 25ABCD specimens mobilized greater q due to the generation of smaller Δu, which became negative at ε_a of about 5%. However, at

J. Geotech. Geoenviron. Eng., 2023, 149(5): 04023019

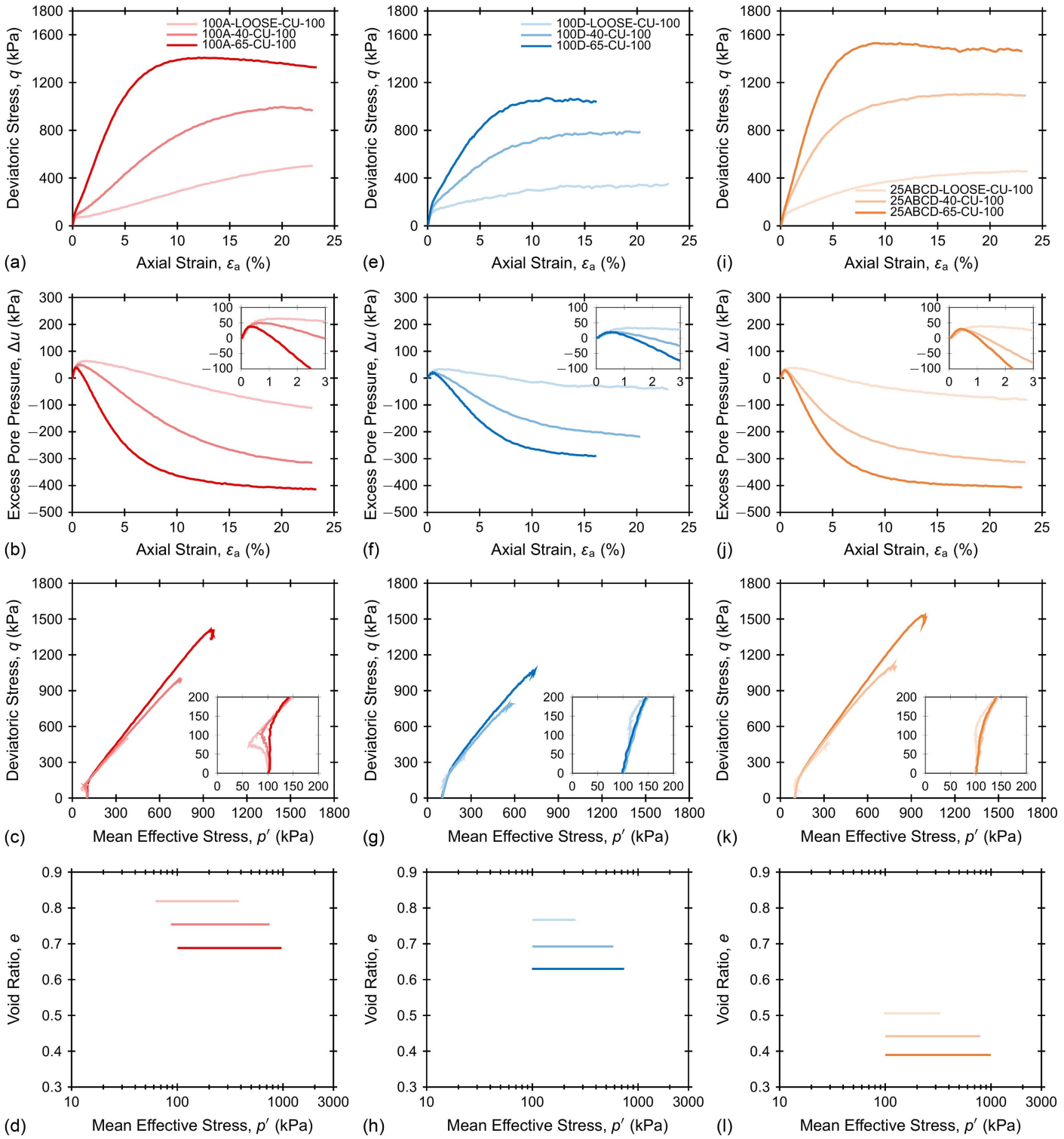

Fig. 7. ICU test results for specimens of (a–d) 100A; (e–h) 100D; and (i–l) 25ABCD at different D_R and $\sigma'_{3c} = 100$ kPa.

ε_a greater than about 17%, the magnitude of Δu was greater for the 100A specimen, resulting in a slightly greater deviatoric stress. The effective stress paths for the 12CU and 25ABCD specimens show no or little decrease in p', whereas the specimens of 100A and 33ABC initially tracked leftward ($\Delta p' < 0$), then exhibited a phase transformation ($\Delta p' = 0$) after which the mean effective stress continued to increase [Fig. 13(c)].

Figs. 13(e–h) present the undrained test results on the dense 100A, 100B, 100C, 33ABC, and 25ABCD specimens. As shown by the q-ε_a curves, all the specimens exhibited a strain-hardening behavior, and the 25ABCD specimen mobilized the greatest deviatoric stress. All the specimens generated a small initial positive excess pore pressure, followed by negative excess pore pressure, which resulted in the greatest p' values [Figs. 13(f–h)]. The specimens of 100A and 25ABCD generated the greatest negative excess pore pressures compared with those of other soils. The effective stress paths of all the specimens tracked rightward, exhibiting no phase transformation [Fig. 13(g)].

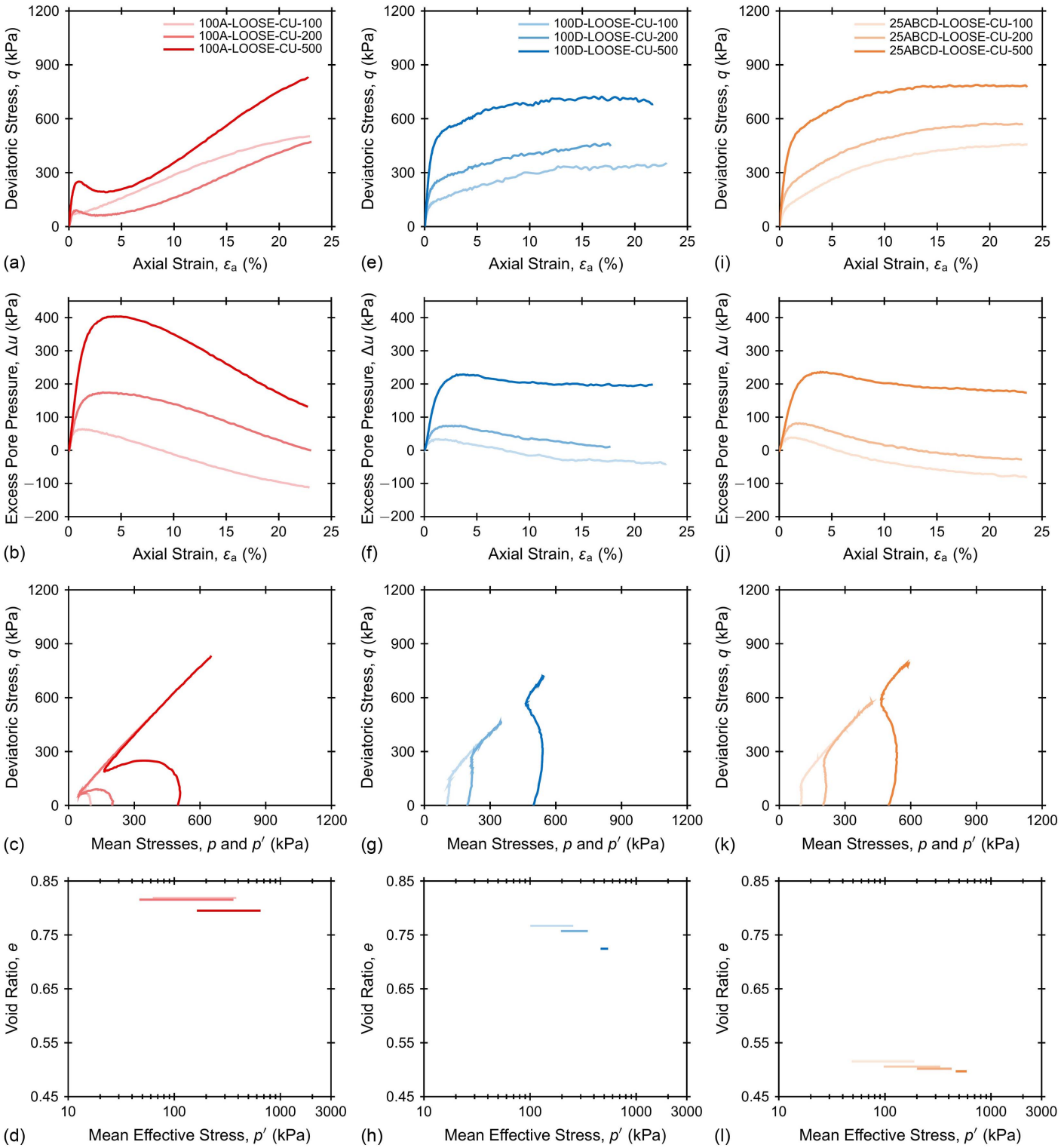

Fig. 8. ICU test results for loose specimens of (a–d) 100A; (e–h) 100D; and (i–l) 25ABCD at different σ'_{3c}.

Mobilized Peak Friction Angle and Maximum Dilation Angle

The effect of gradation and mean particle size on the peak friction angle (ϕ'_{peak}) and maximum dilation angle (ψ_{max}) of the ICD tests were examined in terms of the state parameter. Here, the peak friction angle was calculated using the maximum stress ratio ($\eta_{max} = q/p'$), as follows:

$$\phi'_{peak} = \sin^{-1}\left(\frac{3\eta_{max}}{6+\eta_{max}}\right) \quad (2)$$

The maximum dilation angle in triaxial conditions was estimated using the following equation proposed by Vaid and Sasitharan (1992):

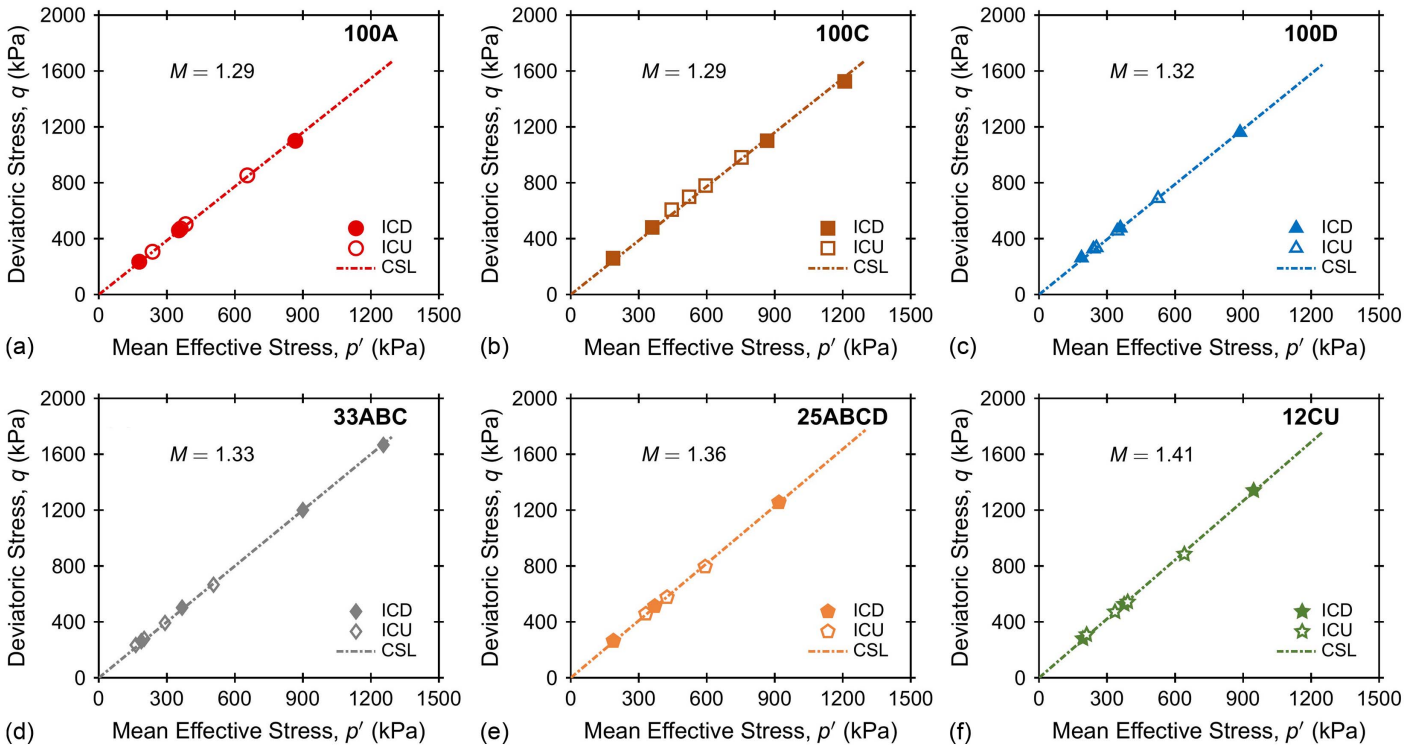

Fig. 9. Critical state lines in q-p' space: (a) 100A; (b) 100C; (c) 100D; (d) 33ABC; (e) 25ABCD; and (f) 12CU.

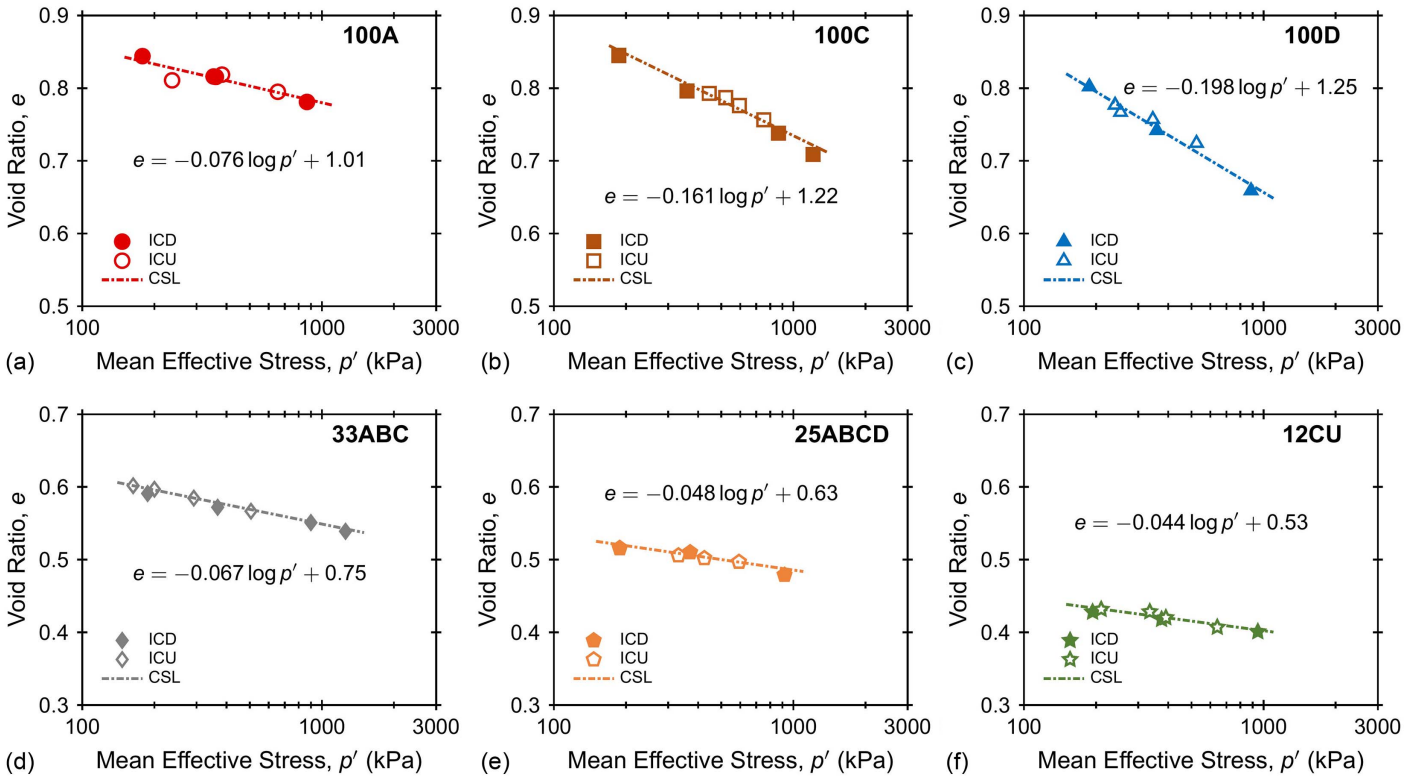

Fig. 10. Critical state lines in e-log p' space: (a) 100A; (b) 100C; (c) 100D; (d) 33ABC; (e) 25ABCD; and (f) 12CU.

$$\psi_{\max} = \sin^{-1}\left(\frac{2}{\frac{3}{|d\varepsilon_v/d\varepsilon_a|_{\max}} - 1}\right) \tag{3}$$

where $|d\varepsilon_v/d\varepsilon_a|_{\max}$ = maximum rate of volume change or dilation.

Fig. 14 shows the variation of ϕ'_{peak} with ξ for drained tests. As expected, ϕ'_{peak} increased as ξ became more negative for all the soils. Also, a greater ϕ'_{peak} was observed for the specimens of well-graded soils (i.e., 33ABC, 25ABCD, and 12CU) compared with those of poorly graded soils (i.e., 100A, 100C, and 100D) at similar

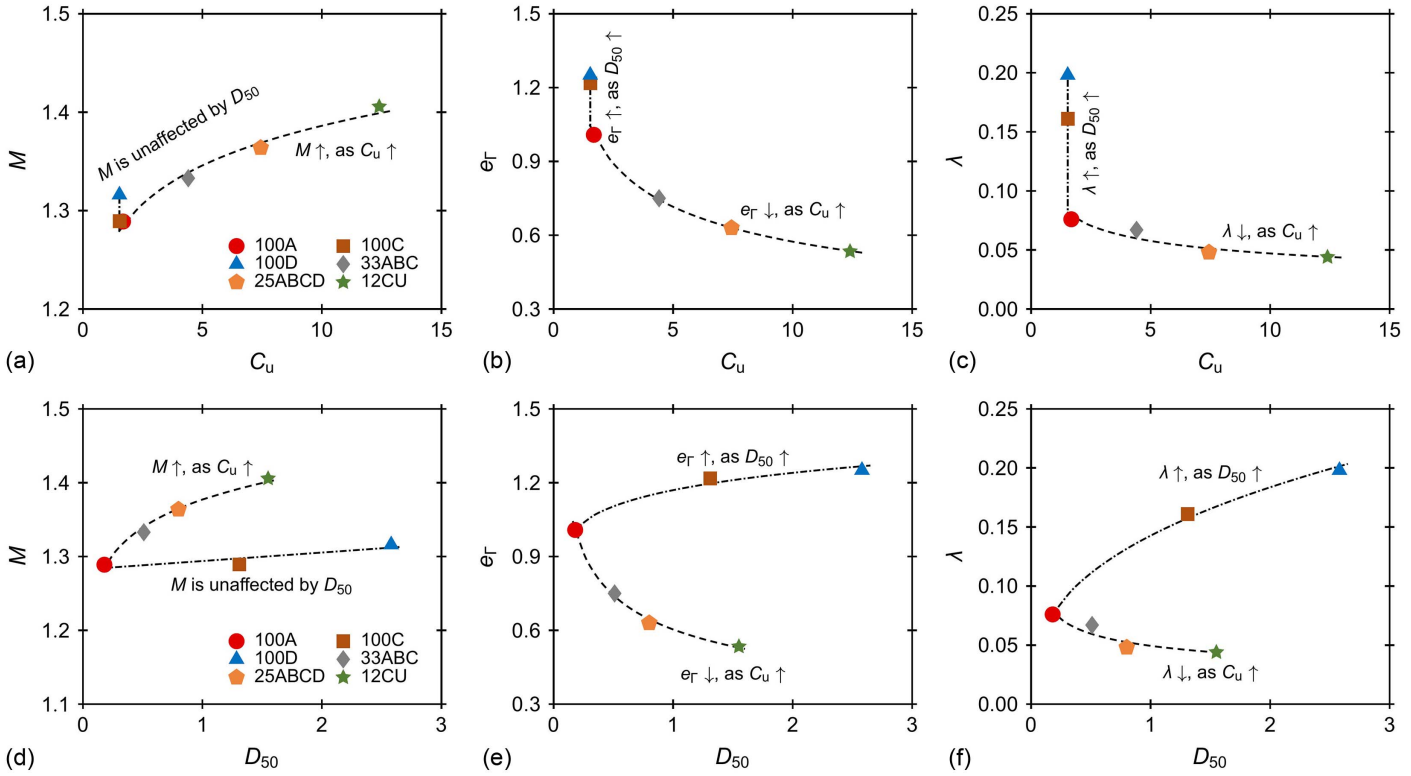

Fig. 11. Variation of M, e_Γ, and λ with (a–c) C_u; and (d–f) D_{50}.

initial state parameters. This difference is due in part to the greater ϕ'_{cs} for the well-graded soils as well as to the greater rate of dilation at any given state parameter, in agreement with results from Simoni and Houlsby (2006). These results contrast to the direct shear results presented by Harehdasht et al. (2018), who made comparisons based on a constant D_R value. However, such a comparison does not account for the effects of D_{50} in the intercept and slope of the CSL, as shown in Figs. 10(a–c). The 100A soil exhibited greater ϕ'_{peak} for a given ξ among the poorly graded soils, suggesting a slight effect of particle size.

Combining the data of both drained and undrained tests, an empirical equation was developed by regression analysis to obtain ϕ'_{peak} as a function of ξ, C_u, and D_{50} and is expressed

$$\phi'_{\text{peak}} = \phi'_{cs} - k\xi$$

$$k = 34(C_u)^{0.285}(D_{50})^{-0.115} \tag{4}$$

As shown in Eq. (4), k is a parameter dependent on both C_u and D_{50}. The value of k increases as C_u is increased and decreases as D_{50} is increased. As shown, the effect of C_u was more pronounced than that of D_{50} based on the power of the corresponding terms.

Fig. 15(a) shows the variation of maximum dilation angle ($\psi_{\max}$) with initial state parameter. As shown, $\psi_{\max}$ increased as ξ becomes more negative for all the soil specimens. The 12CU and 25ABCD soils exhibited the greatest $\psi_{\max}$ at a given ξ in comparison with the poorly graded soils. Of the poorly graded soils, 100A exhibited the greatest $\psi_{\max}$ at a given ξ, in agreement with the ϕ'_{peak} results shown in Fig. 14.

The variation of ϕ'_{peak} with D_R for drained tests is shown in Fig. S6, and the variation of $\psi_{\max}$ with D_R for drained tests is shown in Fig. S7(a). As shown, ϕ'_{peak} generally increased as D_R increased for all the soil specimens. However, no specific trend regarding the effects of C_u and D_{50} on ϕ'_{peak} was observed for the different soils at similar D_R. Similar observations can be made regarding the variation of $\psi_{\max}$ with D_R. This comparison indicates that although the D_R can capture the general trends in ϕ'_{peak} and $\psi_{\max}$, it does not differentiate between soils of different gradation or particle size. This is likely because the D_R parameter contains no information regarding the influence of effective stress, which is an important consideration as shown, for example, in the differences in the intercept and slope of the CSL [Figs. 11(b, c, e, and f)].

Fig. 15(b) shows the variation of $\phi'_{\text{peak}} - \phi'_{cs}$ with ξ along with the mean trends from Been and Jefferies (1985). As shown, the test results exhibited relatively satisfactory agreement with the mean trends, indicating higher strengths and maximum dilation as ξ became more negative. Although some scatter in the data exist, the results generally indicated larger $\phi'_{\text{peak}} - \phi'_{cs}$ for the same ξ for soils with broader gradation, which is consistent with the observations in Fig. 14. Fig. S7(b) shows the variation of $\phi'_{\text{peak}} - \phi'_{cs}$ with D_R, where $\phi'_{\text{peak}} - \phi'_{cs}$ generally increased as D_R increased. However, significant variability was observed when D_R was smaller than 40%, and the data showed no specific trend regarding the effects of C_u and D_{50} on $\phi'_{\text{peak}} - \phi'_{cs}$ for the specimens prepared at similar D_R.

Stress-Dilatancy Behavior

Rowe (1962) developed a stress-dilatancy relationship, which was later modified by Bolton (1986) with a scalar correction (b) that accounts for energy losses and adjusts for differences between various shearing modes. The Rowe (1962) stress-dilatancy relationship can be expressed

$$R = D\tan^2\left(\frac{\pi}{4} + \frac{\phi'_{cs}}{2}\right) \tag{5}$$

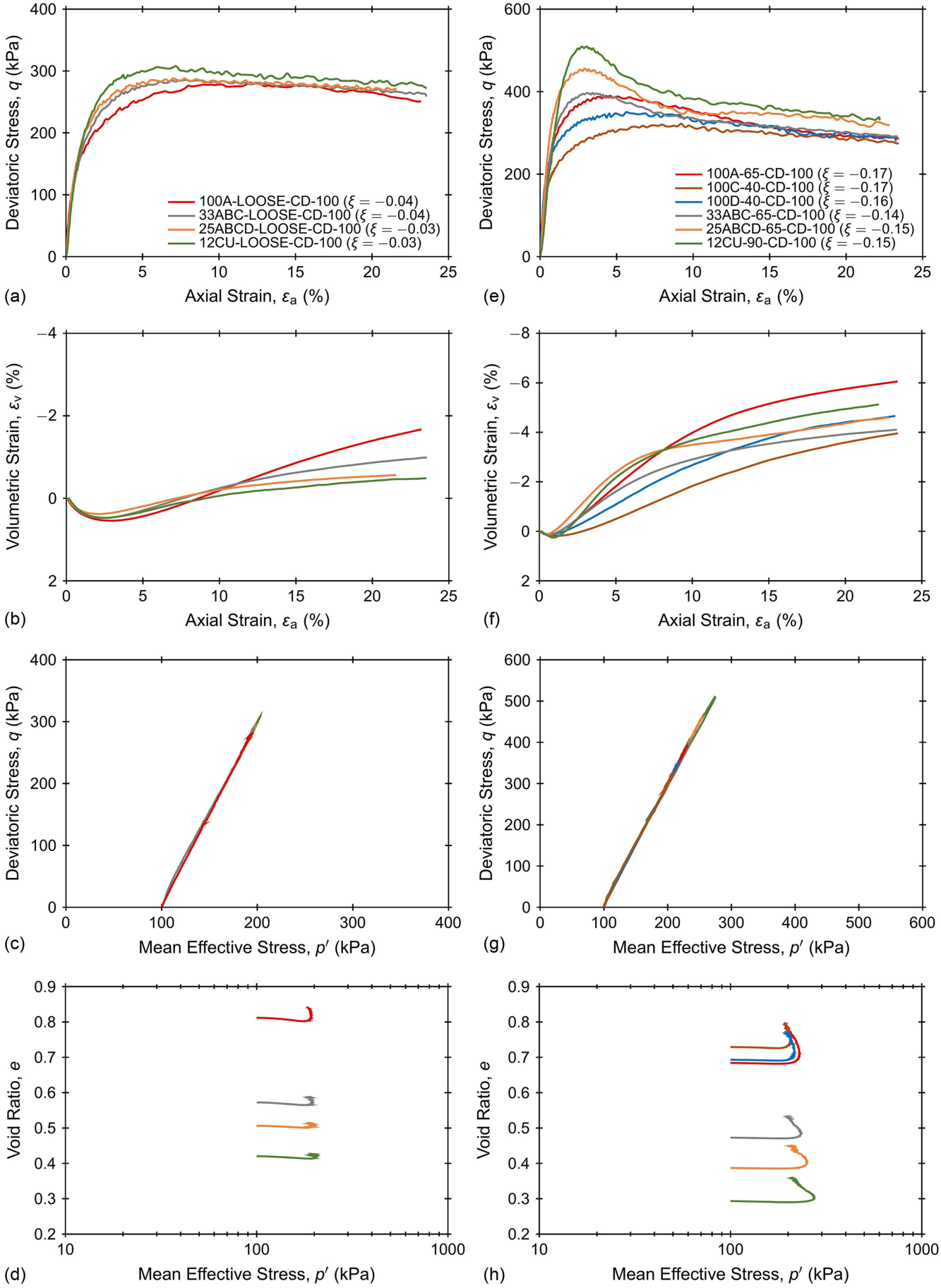

Fig. 12. Drained test results for (a–d) $\xi = -0.03 \pm 0.01$; and (e–h) $\xi = -0.16 \pm 0.02$.

J. Geotech. Geoenviron. Eng., 2023, 149(5): 04023019

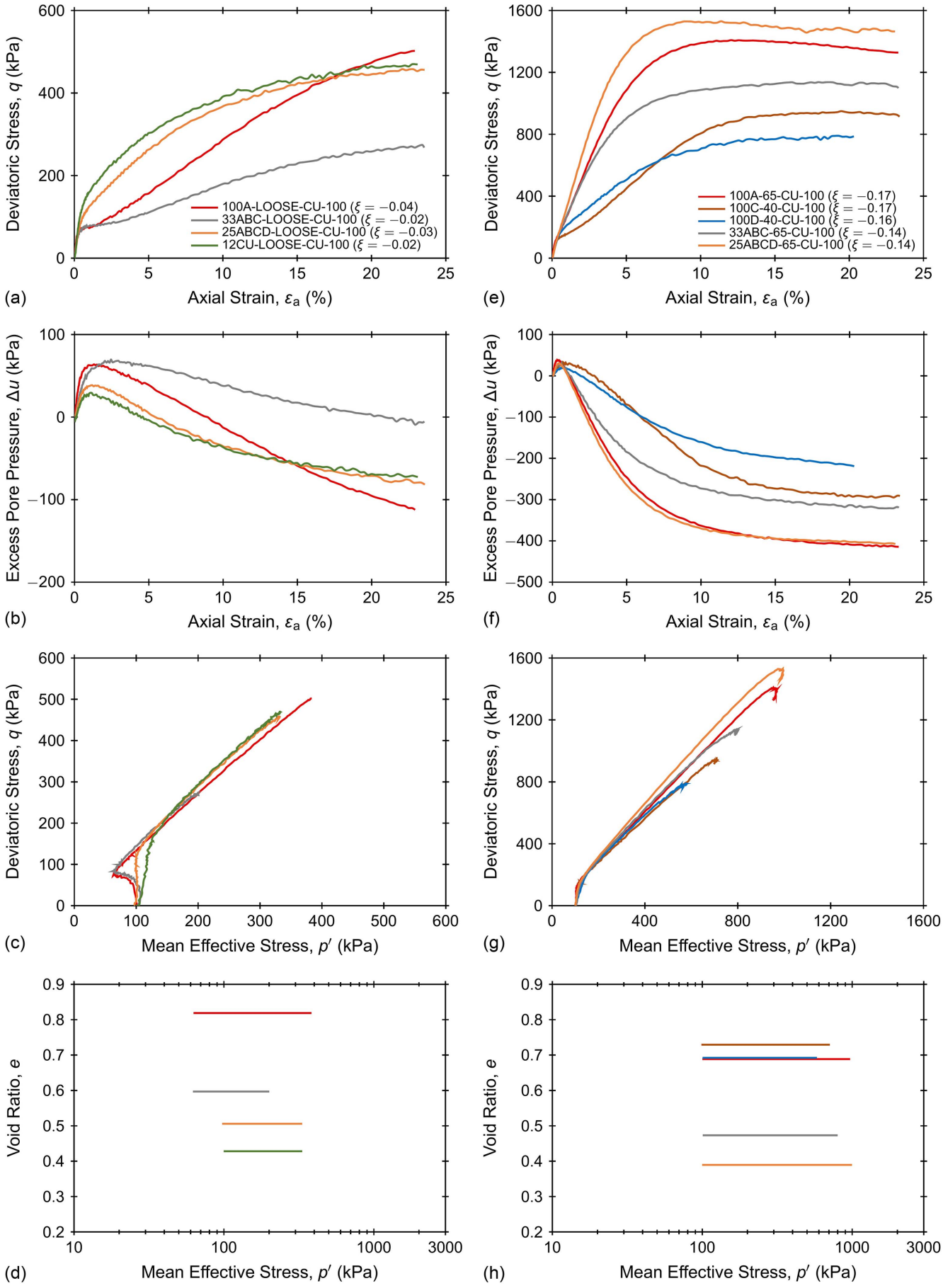

Fig. 13. Undrained test results for (a–d) $\xi = -0.03 \pm 0.01$; and (e–h) $\xi = -0.16 \pm 0.02$.

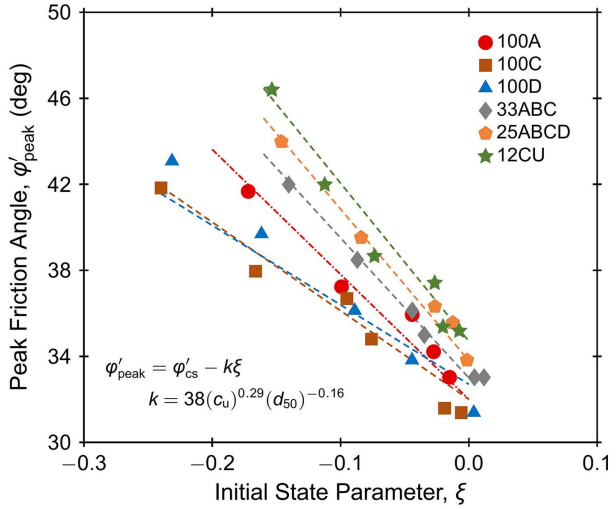

Fig. 14. Variation of ϕ'_{peak} with ξ for drained tests.

where $R = \sigma'_1/\sigma'_3$ is the effective principal stress ratio; and $D = 1 - d\varepsilon_v/d\varepsilon_a$ is the dilatancy. The Bolton (1986) expression can be expressed

$$\phi'_{max} - \phi'_{cs} = b \cdot \psi_{max} \tag{6}$$

where a b-value of 0.8 for plane-strain conditions was proposed based on 17 experimental data sets of poorly graded sands with a narrow range of gradations ($C_u < 1.9$); others have proposed b-values in the range of 0.3 to 0.6 for triaxial compression conditions (e.g., Chakraborty and Salgado 2010). Bolton (1986) also stated that the effect of state is strongly correlated with soil strength, which is in turn related to the effects of particle size, shape, and gradation. Because the current stress-dilatancy framework does not account for the effects of particle size and gradation, a discussion on the effect of these parameters is presented herein.

Fig. 16(a) shows the relationship between ϕ'_{peak}-ϕ'_{cs} and ψ_{max} (i.e., the stress-dilatancy relationship) for all the soils tested in this study, obtained from the drained tests. As shown, no significant effect of D_{50} and C_u was observed, suggesting that the contribution of dilation to the friction angle in excess of the critical state value is unaffected by these parameters. The fitted trend to data for all soils indicated an average b-value of 0.54. Based on triaxial and direct shear tests, Harehdasht et al. (2017, 2018) also found no effect of C_u on the b-value of Eq. (6). However, they reported a decrease in the b-value with increasing D_{50}; as mentioned previously, this trend was not found in the results presented here. The source of this difference is unknown, but may be due to the testing device and methods used or the interpretation methods used and associated assumptions.

The drained test results for specimens of all soils are plotted in Fig. 16(b) as $\phi'_{peak} - \phi'_{cs}$ versus mean effective stress at failure (p'_f) (i.e., at peak q) to compare with the relationships proposed by Bolton (1986). Empirical trend lines corresponding to relative densities (D_R) of 25%, 40%, 65%, and 100% are also shown using Bolton (1986) relationship, defined as follows:

$$I_R = D_R(Q - \ln p'_f) - R \tag{7}$$

where Q and R = material constants taken as 10 and 1, respectively, based on Bolton's recommendations for quartz sands; p'_f is in kPa; and I_R = relative density index that relates the peak and critical state friction angles as follows:

$$\phi'_{peak} - \phi'_{cs} = 3I_R \tag{8}$$

The trend lines rotate upward for denser soils, corresponding to a more dilative behavior that shifts the mobilized peak friction angle further from the critical state. As shown, the specimens of all the soils prepared for a relative density less than 30% generally plotted between expected D_R values (i.e. $D_{R,Bolton}$) of 25% and 40% based on the Bolton (1986) relationship. The specimens prepared at a D_R of 40% plotted at expected densities between 55% and 75% D_R based on Eq. (7). The specimens prepared at a target D_R of 65% plotted at expected D_R values between 80% and 90%, and the only very dense specimen of 12CU prepared at a D_R of about 90% plotted above the $D_R = 100\%$ line. The disparity between the experimental results and those predicted by Eq. (7) may be attributed to the angular shape of the soil particles used in this study, which would contribute to a more dilative soil response for a given D_R than the outwash and river sands evaluated in the Bolton (1986) framework. A similar disparity between experimentally measured values and those predicted by Eq. (7) were reported by Simoni and Houlsby (2006) based on direct shear tests.

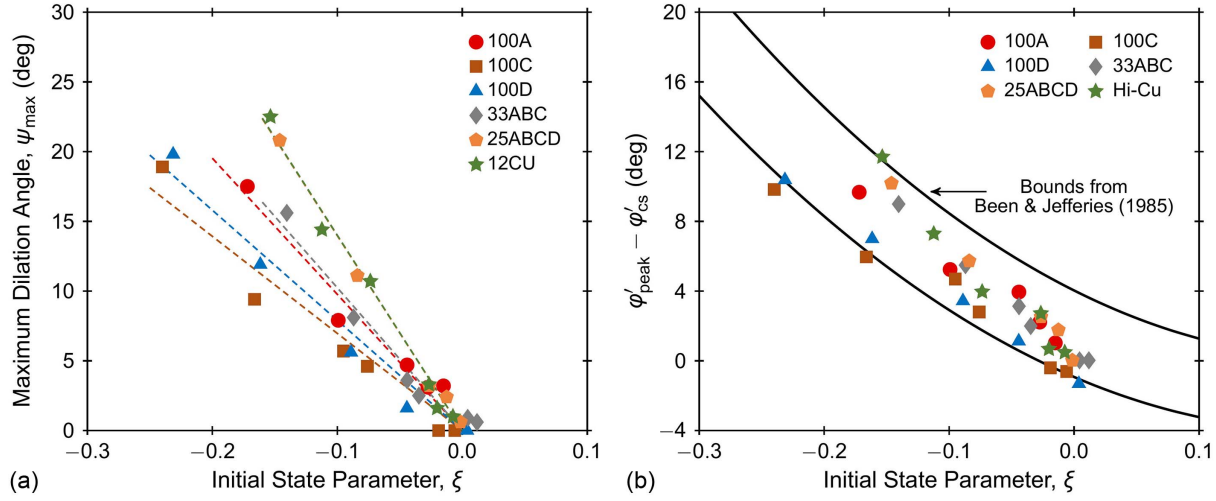

Fig. 15. (a) Variation of ψ_{max}; and (b) ϕ'_{peak}-ϕ'_{cs} with ξ.

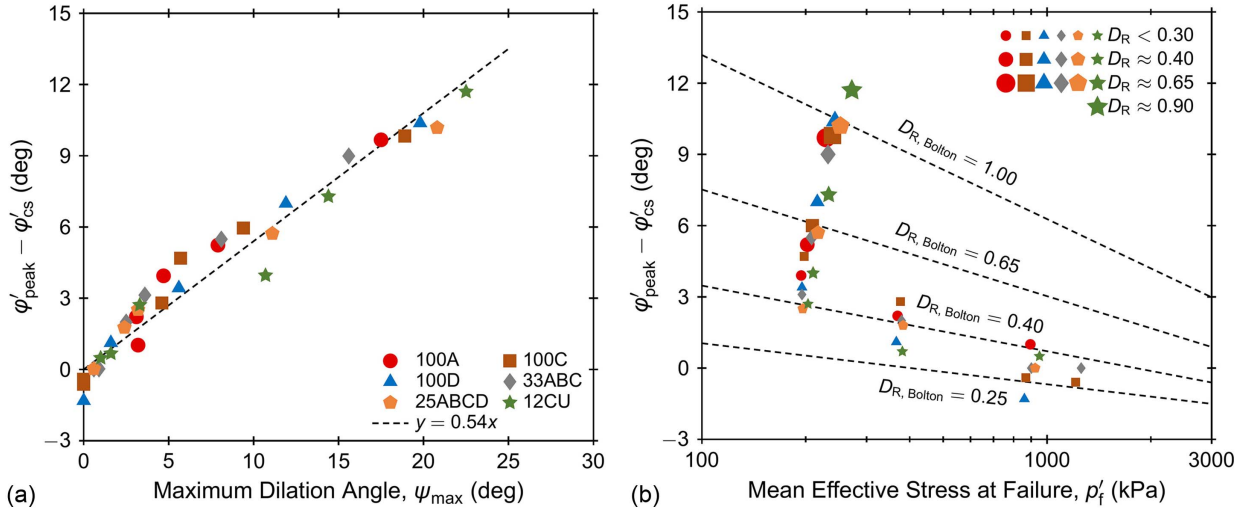

Fig. 16. Relation between (a) ϕ'_{peak}-ϕ'_{cs} and ψ_{max}; and (b) ϕ'_{peak}-ϕ'_{cs} and p'_f.

The effect of D_{50} and C_u on the loose specimens ($D_R < 30\%$) is not clearly pronounced [Fig. 16(b)]. However, for the medium-dense ($D_R \approx 40\%$) and dense ($D_R \approx 65\%$) specimens, increasing D_{50} and C_u resulted in higher peak friction angles that further deviated from Bolton's equation. For instance, at a $D_R \approx 40\%$ the $\phi'_{peak} - \phi'_{cs}$ values for the 100D, 100C, and 100A specimens were 6.9°, 6.0°, and 5.1°, respectively. Also, the $\phi'_{peak} - \phi'_{cs}$ values of the 12CU, 25ABCD, and 33ABC specimens at a $D_R \approx 40\%$ were 7.3°, 5.8°, and 5.5°. Similar trends were observed for the specimens prepared at a target D_R of 65%. Hence, the soil specimens with higher D_{50} and C_u exhibited greater ϕ'_{peak} in comparison with their corresponding ϕ'_{cs} and a more dilative soil response, resulting in significant deviations from the Bolton (1986) framework [i.e., Eq. (7)].

Magnitude and Rate of Excess Pore Pressure Generation

The development of shear-induced excess pore pressure during undrained shearing is related to the dilative or contractive tendencies of a soil specimen. The greatest magnitude of negative excess pore pressure (Δu_{min}), which typically corresponded to the end of test condition, and the greatest rate of negative pore pressure generation $[(\delta u/d\varepsilon_a)_{min}]$ obtained from the undrained tests are shown in Figs. 17(a and b), respectively, as a function of ξ.

As shown, higher negative Δu_{min} was generated as ξ became more negative [Fig. 17(a)]. With regards to the effect of particle size, the specimens with the smallest D_{50} (i.e., 100A) generated the greatest Δu_{min}, whereas the specimens with the largest D_{50} (i.e., 100D) generated the smallest negative Δu_{min} at similar ξ. Although the 100C and 100D poorly graded soils generated smaller magnitudes of Δu_{min} at any given ξ, no systematic difference was observed for the 100A, 33ABC, 25ABCD, and 12CU soils.

Greater magnitudes of $(\delta u/d\varepsilon_a)_{min}$ were observed as ξ became more negative [Fig. 17(b)]. Similar trends were observed with regard to the effect of particle size. Of the poorly graded soils, 100A generated the greatest $(\delta u/d\varepsilon_a)_{min}$ magnitude at any given ξ. The data suggest a slightly greater $(\delta u/d\varepsilon_a)_{min}$ at any given state parameter for the well-graded soils than for the 100A soil, likely due to the more dilative response of the former soils. However, the differences are small and possibly subjected to the effects of experimental variability.

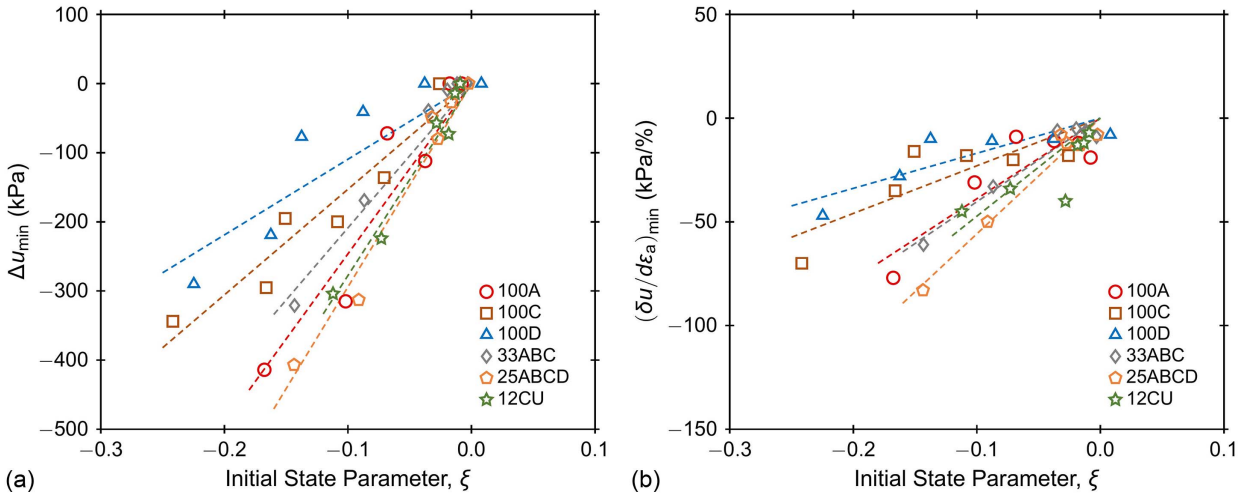

Fig. 17. Variation of (a) Δu; and (b) minimum rate of change of pore pressure with ξ.

J. Geotech. Geoenviron. Eng., 2023, 149(5): 04023019

Figs. S8(a and b) show the variation of $\Delta u_{\min}$ and $(\delta u/\mathrm{d}\varepsilon_a)_{\min}$, respectively, as a function of D_R. As shown, greater negative $\Delta u_{\min}$ and $(\delta u/\mathrm{d}\varepsilon_a)_{\min}$ were generated as D_R increased for all the soil specimens. However, no systematic effect of gradation and particle size on $\Delta u_{\min}$ and $(\delta u/\mathrm{d}\varepsilon_a)_{\min}$ was observed for the specimens prepared at similar D_R. These results further show that the relative density parameter captured the general trend in pore pressure generation and dilatancy behaviors, but did not capture the finer effects of gradation and particle size.

Conclusions

A series of isotropically consolidated drained and undrained triaxial tests were conducted to systematically investigate the effects of mean particle size and gradation on the triaxial compression behavior of well-graded coarse-grained soils. The soils used in this study were sourced from a single deposit to eliminate the effects of particle shape and mineralogy. Tests were performed on pluviated specimens over a range of initial densities and confining stresses.

Both gradation and median particle size had an effect on the attainable void ratios and critical state lines. The index void ratio values ($e_{\max}$ and $e_{\min}$) decreased as the gradation widened (i.e., C_u increased), whereas no significant effect of the median particle size (D_{50}) was observed. The critical state stress ratio (M) in the q-p' plane increased slightly as the range of particle sizes increased, whereas the effect of D_{50} on M was negligible. The intercept of the critical state line in e-log p' space (e_Γ) decreased as C_u was increased, resulting in a downward shift with increasing C_u. Also, e_Γ increased slightly as D_{50} was increased for the poorly graded soils. The slope (λ) of the CSL in e-log p' space decreased as C_u was increased, indicating a decrease in compressibility. However, λ of the poorly graded soils increased as D_{50} was increased.

As the initial state parameter (ξ) of all soils became more negative (i.e., specimens became denser), both the peak friction angle (ϕ'_{peak}) and maximum dilation angle ($\psi_{\max}$) increased. At similar ξ, both ϕ'_{peak} and $\psi_{\max}$ generally increased with increasing gradation. Of the poorly graded soils, the soil with the smallest D_{50} (i.e., 100A) exhibited the greatest ϕ'_{peak} and $\psi_{\max}$. Also, $\phi'_{\text{peak}} - \phi'_{cs}$ tended to increase as the gradation became wider across a range of ξ and confining pressures, and the data showed general agreement with the trends and bounds established by Been and Jefferies (1985). The undrained test results showed that higher negative excess pore pressures ($\Delta u_{\min}$) were generated as ξ became more negative for all the soils. The soils with wider gradation appeared to generate negative excess pore pressures at greater rates $[(\delta u/\mathrm{d}\varepsilon_a)_{\min}]$ for any given ξ. Also, the soil with the smallest D_{50} (i.e., 100A) generated the greatest magnitude of negative excess pore pressures.

The relationship between ϕ'_{peak}-ϕ'_{cs} and $\psi_{\max}$ exhibited no significant effect of either C_u or D_{50}, and fitting all the data resulted in a b-value of 0.54, which is within the typical range for triaxial compression reported in the literature. A comparison of the experimental measurements of ϕ'_{peak}-ϕ'_{cs} with those predicted by the Bolton (1986) equations showed greater measured values for any given relative density (D_R), which may be attributed to the angular shape of the soil particles used in this study compared with the clean river sands evaluated by Bolton (1986).

Overall, the results indicate that although D_R captured the general trends in the strength and dilation parameters [i.e., ϕ'_{peak}, $\psi_{\max}$, ϕ'_{peak}-ϕ'_{cs}, $(\delta u/\mathrm{d}\varepsilon_a)_{\min}$, and $\Delta u_{\min}$] and specimen response, it did not capture the specific effects of C_u and D_{50}, likely because the parameter does not account for the aforementioned differences in the corresponding CSLs.

Data Availability Statement

Some or all data, models, or code generated or used during the study are available in a repository or online in accordance with funder data retention policies at DesignSafe-CI under PRJ-3732 at 10.17603/ds2-crtg-j217.

Acknowledgments

The National Science Foundation (NSF) provided the funding for this work under Grant No. CMMI-1916152 and also funded the Natural Hazards Engineering Research Infrastructure (NHERI) shared use centrifuge facility at the University of California at Davis under Grant No. CMMI-1520581. The authors would also like to thank Katerina Ziotopoulou, Rachel Reardon, Francisco Humire, Mandeep Singh Basson, Nathan Love, Trevor Carey, and Anna Chiaradonna for their insights and recommendations.

Supplemental Materials

Figs. S1–S8 are available online in the ASCE Library (www.ascelibrary.org).

References

Altuhafi, F. N., and M. R. Coop. 2011. "Changes to particle characteristics associated with the compression of sands." *Géotechnique* 61 (6): 459–471. https://doi.org/10.1680/geot.9.P.114.

ASTM. 2016a. *Standard test methods for maximum index density and unit weight of soils using a vibratory table*. D4253-16. West Conshohocken, PA: ASTM.

ASTM. 2016b. *Standard test methods for minimum index density and unit weight of soils and calculation of relative density.* D4254-16. West Conshohocken, PA: ASTM.

Been, K., and M. G. Jefferies. 1985. "A state parameter for sands." *Géotechnique* 35 (2): 99–112. https://doi.org/10.1680/geot.1985.35.2.99.

Bishop, A. W. 1954. "The pore pressure coefficients A and B." *Géotechnique* 4 (4): 143–147. https://doi.org/10.1680/geot.1954.4.4.143.

Bolton, M. D. 1986. "The strength and dilatancy of sands." *Géotechnique* 36 (1): 65–78. https://doi.org/10.1680/geot.1986.36.1.65.

Carey, J. T., A. Chiaradonna, N. C. Love, D. W. Wilson, K. Ziotopoulou, A. Martinez, and J. T. DeJong. 2022. "Effect of soil gradation on embankment response during liquefaction: A centrifuge testing program." *Soil Dyn. Earth. Eng.* 157: 107221. https://doi.org/10.1016/j.soildyn.2022.107221.

Chakraborty, T., and R. Salgado. 2010. "Dilatancy and shear strength of sand at low confining pressures." *J. Geotech. Geoenviron. Eng.* 136 (3): 527–532. https://doi.org/10.1061/(ASCE)GT.1943-5606.0000237.

Chang, N. Y., and H. Y. Ko. 1982. *Effects of grain size distribution on dynamic properties and liquefaction potential of granular soils*. NSF Rep. No. R82-103. Washingtgn, DC: Directorate for Engineering National Science Foundation.

Daniel, C. R., J. A. Howie, R. G. Campanella, and A. Sy. 2004. "Characterization of SPT grain size effects in gravels." In *Proc., 2nd Int. Conf. on Site Characterization (ISC'2)*. Rotterdam, Netherlands: Millpress.

De Josselin de Jong, G. 1976. "Rowe's stress-dilatancy relation based on friction." *Géotechnique* 26 (3): 527–534. https://doi.org/10.1680/geot.1976.26.3.527.

Deng, Y., Y. Yilmaz, A. Gokce, and C. S. Chang. 2021. "Influence of particle size on the drained shear behavior of a dense fluvial sand." *Acta Geotech.* 16 (7): 2071–2088. https://doi.org/10.1007/s11440-021-01143-7.

Evans, M. D., and S. Zhou. 1995. "Liquefaction behavior of sand-gravel composites." *J. Geotech. Eng.* 121 (3): 287–298. https://doi.org/10.1061/(ASCE)0733-9410(1995)121:3(287).

Fragaszy, R. J., W. Su, and F. H. Siddiqi. 1990. "Effects of oversize particles on the density of clean granular soils." *Geotech. Test. J.* 13 (2): 106–114. https://doi.org/10.1520/GTJ10701J.

Fragaszy, R. J., W. Su, F. H. Siddiqi, and C. L. Ho. 1992. "Modeling strength of sandy gravel." *J. Geotech. Eng. Div.* 118 (6): 920–935. https://doi.org/10.1061/(ASCE)0733-9410(1992)118:6(920).

Goto, S., S. Nishio, and Y. Yoshimi. 1994. "Dynamic properties of gravels sampled by ground freezing." In *Ground failures under seismic conditions*, 141–157. New York: ASCE.

Gudehus, G. 1996. "A comprehensive constitutive equation for granular materials." *Soils Found.* 36 (1): 1–12. https://doi.org/10.3208/sandf.36.1.

Guo, P., and X. Su. 2007. "Shear strength, interparticle locking, and dilatancy of granular materials." *Can. Geotech. J.* 44 (5): 579–591. https://doi.org/10.1139/t07-010.

Harehdasht, S. A., M. N. Hussien, M. Karray, V. Roubtsova, and M. Chekired. 2018. "Influence of particle size and gradation on shear strength–dilation relation of granular materials." *Can. Geotech. J.* 56 (2): 208–227. https://doi.org/10.1139/cgj-2017-0468.

Harehdasht, S. A., M. Karray, M. N. Hussien, and M. Chekired. 2017. "Influence of particle size and gradation on the stress-dilatancy behavior of granular materials during drained triaxial compression." *Int. J. Geomech.* 17 (9): 04017077. https://doi.org/10.1061/(ASCE)GM.1943-5622.0000951.

Houlsby, G. T. 1991. "How the dilatancy of soils affects their behavior." In Vol. 4 of *Proc. 10th European Conf. on Soil Mechanics and Foundation Engineering*, 1189–1202. Rotterdam, Netherlands: Balkema.

Humire, F. A. 2022. "Liquefaction and post-liquefaction behavior of coarse-grained soils." Ph.D. dissertation, Dept. of Civil and Environmental Engineering, Univ. of California, Davis.

Jiang, M. D., Z. X. Yang, and Y. H. Xie. 2018. "The influence of particle-size distribution on critical state behavior of spherical and non-spherical particle assemblies." *Granular Matter* 20 (Nov): 1–15. https://doi.org/10.1007/s10035-018-0850-x.

Kokusho, T., and Y. Tanaka. 1994. "Dynamic properties of gravel layers investigated by in-situ freezeing sampling." In *Ground failures under seismic conditions*, 121–140. New York: ASCE.

Kokusho, T., and Y. Yoshida. 1997. "SPT N-value and S-wave velocity for gravelly soils with different grain size distribution." *Soils Found.* 37 (4): 105–113. https://doi.org/10.3208/sandf.37.4_105.

Kramer, S. L., N. Sivaneswaran, and R. O. Davis. 1990. "Analysis of membrane penetration in triaxial test." *J. Eng. Mech.* 116 (4): 773–789. https://doi.org/10.1061/(ASCE)0733-9399(1990)116:4(773).

Lagioia, R., A. Sanzeni, and F. Colleselli. 2006. "Air, water and vacuum pluviation of sand specimens for the triaxial apparatus." *Soils Found.* 46 (1): 61–67. https://doi.org/10.3208/sandf.46.61.

Lee, K. L., and H. Seed. 1967. "Drained strength characteristics of sands." *J. Soil Mech. Found. Div.* 93 (6): 117–141. https://doi.org/10.1061/JSFEAQ.0001048.

Li, G., Y. J. Liu, C. Dano, and P. Y. Hicher. 2015. "Grading-dependent behavior of granular materials: From discrete to continuous modeling." *J. Eng. Mech.* 141 (6): 04014172. https://doi.org/10.1061/(ASCE)EM.1943-7889.0000866.

Liu, D., C. O'Sullivan, and J. A. H. Carraro. 2021. "Influence of particle size distribution on the proportion of stress-transmitting particles and implications for measures of soil state." *J. Geotech. Geoenviron. Eng.* 147 (3): 04020182. https://doi.org/10.1061/(ASCE)GT.1943-5606.0002466.

Liu, Y., G. Li, Z. Yin, C. Dano, P. Hicher, X. Xia, and J. Wang. 2014. "Influence of grading on the undrained behavior of granular materials." *C. R. Mec.* 342 (2): 85–95. https://doi.org/10.1016/j.crme.2013.11.001.

Menq, F.-Y. 2003. "Dynamic properties of sandy and gravelly soils." Ph.D. dissertation, Dept. of Civil, Environmental, and Architectural Engineering, Univ. of Texas at Austin.

Miura, S., and S. Toki. 1982. "A sample preparation method and its effect on static and cyclic deformation-strength properties of sand." *Soils Found.* 22 (1): 61–77. https://doi.org/10.3208/sandf1972.22.61.

Nakai, T. 1997. "Dilatancy characteristics of geomaterials." In *Deformation and progressive failure in geomaterials, IS-Nagoya'97*, edited by A. Asaoka, T. Adachi, and F. Oda, 899–906. Amsterdam, Netherlands: Elsevier.

Negussey, D., W. K. D. Wijewickreme, and Y. P. Vaid. 1988. "Constant volume friction angle of granular materials." *Can. Geotech. J.* 25 (1): 50–55. https://doi.org/10.1139/t88-006.

Newland, P. L., and B. H. Allely. 1957. "Volume changes in drained triaxial tests on granular materials." *Géotechnique* 7 (1): 17–34. https://doi.org/10.1680/geot.1957.7.1.17.

Pires-Sturm, A. P., and J. T. DeJong. 2022. "Influence of particle size and gradation on liquefaction potential and dynamic response." *J. Geotech. Geoenviron. Eng.* 148 (6): 04022045. https://doi.org/10.1061/(ASCE)GT.1943-5606.0002799.

Pradhan, T. B. S., F. Tatsuoka, and Y. Sato. 1989. "Experimental stress dilatancy relations of sand subjected to cyclic loading." *Soils Found.* 29 (1): 45–64. https://doi.org/10.3208/sandf1972.29.45.

Reynolds, O. 1885. "On the dilatancy of media composed of rigid particles in contact." *Philos. Mag.* 5 (127): 469–481. https://doi.org/10.1080/14786448508627791.

Rowe, P. W. 1962. "The stress-dilatancy relation for static equilibrium of an assembly of particles in contact." *Proc. R. Soc. London, Ser. A.* 269 (1339): 500–527. https://doi.org/10.1080/14786448508627791.

Rowe, P. W. 1969. "The relation between the shear strength of sands in triaxial compression, plane strain and direct shear." *Géotechnique* 19 (1): 75–86. https://doi.org/10.1680/geot.1969.19.1.75.

Santamarina, J. C., K. A. Klein, and M. A. Fam. 2001. *Soils and waves—Particulate materials behavior.* New York: Wiley.

Sawyer, B. D. 2020. "Cone penetration testing of coarse-grained soils in the centrifuge to examine the effects of soil gradation and centrifuge scaling." M.S. thesis, Dept. of Civil and Environmental Engineering, Univ. of California, Davis.

Schofield, A. N., and C. P. Wroth. 1968. *Critical state soil mechanics*. London: McGraw-Hill.

Simoni, A., and G. T. Houlsby. 2006. "The direct shear strength and dilatancy of sand-gravel mixtures." *Geotech. Geol. Eng.* 24 (3): 523–549. https://doi.org/10.1007/s10706-004-5832-6.

Singh, S., H. B. Seed, and C. K. Chan. 1982. "Undisturbed sampling of saturated sands by freezing." *J. Geotech. Eng. Div.* 108 (2): 247–264. https://doi.org/10.1061/AJGEB6.0001242.

Skempton, A. W., and A. W. Bishop. 1950. "The measurement of the shear strength of soils." *Géotechnique* 2 (2): 90–108. https://doi.org/10.1680/geot.1950.2.2.90.

Sturm, A. P. 2019. "On the liquefaction potential of gravelly soils: Characterization, triggering and performance." Ph.D. dissertation, Dept. of Civil and Environmental Engineering, Univ. of California, Davis.

Taylor, D. W. 1948. *Fundations of Soil Mechanics*. New York: Wiley.

Torres-Cruz, L. A., and J. C. Santamarina. 2020. "The critical state line of nonplastic tailings." *Can. Geotech. J.* 57 (10): 1508–1517. https://doi.org/10.1139/cgj-2019-0019.

Vaid, Y. P., and D. Negussey. 1984. "Relative density of pluviated sand samples." *Soils Found.* 24 (2): 101–105. https://doi.org/10.3208/sandf1972.24.2_101.

Vaid, Y. P., and S. Saivathayalan. 2000. "Fundamental factors affecting liquefaction susceptibility of sands." *Can. Geotech. J.* 37 (3): 592–606. https://doi.org/10.1139/t00-040.

Vaid, Y. P., and S. Sasitharan. 1992. "The strength and dilatancy of sand." *Can. Geotech. J.* 29 (3): 522–526. https://doi.org/10.1139/t92-058.

Vaid, Y. P., S. Sivathayalan, and D. Stedman. 1999. "Influence of specimen-reconstituting method on the undrained response of sand." *Geotech. Test. J.* 22 (3): 187–195. https://doi.org/10.1520/GTJ11110J.

Voivret, C., F. Radjai, J. Y. Delenne, and M. S. El Youssoufi. 2009. "Multiscale force networks in highly polydisperse granular media." *Phys. Rev. Lett.* 102 (17): 178001. https://doi.org/10.1103/PhysRevLett.102.178001.

Wan, R. G., and P. J. Guo. 1998. "A simple constitutive model for granular soils: Modified stress-dilatancy approach." *Comput. Geotech.* 22 (2): 109–133. https://doi.org/10.1016/S0266-352X(98)00004-4.

Wan, R. G., and P. J. Guo. 1999. "A pressure and density dependent dilatancy model for granular materials." *Soils Found.* 39 (6): 1–11. https://doi.org/10.3208/sandf.39.6_1.

Wang, Z.-L., Y. F. Dafalias, X.-S. Li, and F. L. Makdisi. 2002. "State pressure index for modelling sand behavior." *J. Geotech. Geoenviron. Eng.*

128 (6): 511–519. https://doi.org/10.1061/(ASCE)1090-0241(2002)128:6(511).
Wood, D. M., and K. Maeda. 2008. "Changing grading of soil: Effect on critical states." *Acta Geotech.* 3 (Mar): 3–14. https://doi.org/10.1007/s11440-007-0041-0.
Yan, W. M., and J. Dong. 2011. "Effect of particle grading on the response of an idealized granular assemblage." *Int. J. Geomech.* 11 (4): 276–285. https://doi.org/10.1061/(ASCE)GM.1943-5622.0000085.
Yang, J., and X. S. Li. 2004. "State-dependent strength of sands from the perspective of unified modeling." *J. Geotech. Geoenviron. Eng.* 130 (2): 186–198. https://doi.org/10.1061/(ASCE)1090-0241(2004)130:2(186).
Yang, J., and X. D. Luo. 2015. "Exploring the relationship between critical state and particle shape for granular materials." *J. Mech. Phys. Solids* 84 (Nov): 196–213. https://doi.org/10.1016/j.jmps.2015.08.001.
Yang, J., and X. D. Luo. 2017. "The critical state friction angle of granular materials: Does it depend on grading?" *Acta Geotech.* 13 (3): 535–547. https://doi.org/10.1007/s11440-017-0581-x.
Yi, L. Y., K. J. Dong, R. P. Zou, and A. B. Yu. 2011. "Coordination number of the packing of ternary mixtures of spheres: DEM simulations versus measurements." *Ind. Eng. Chem. Res.* 50 (14): 8773–8785. https://doi.org/10.1021/ie200765h.
Yoshimi, Y., K. Tokimatsu, and J. Ohara. 1994. "In situ liquefaction resistance of clean sands over a wide density range." *Géotechnique* 44 (3): 479–494. https://doi.org/10.1680/geot.1994.44.3.479.
Youd, T. L. 1973. "Factors controlling maximum and minimum densities of sands." *Evaluation of relative density and its role in geotechnical projects involving cohesionless soils*, 98–112. West Conshohocken, PA: ASTM.
Zhang, J., S. C. R. Lo, M. M. Rahman, and J. Yan. 2018. "Characterizing monotonic behavior of pond ash within critical state approach." *J. Geotech. Geoenviron. Eng.* 144 (1): 04017100. https://doi.org/10.1061/(ASCE)GT.1943-5606.0001798.
Zheng, J., and R. D. Hryciw. 2015. "Traditional soil particle sphericity, roundness and surface roughness by computational geometry." *Géotechnique* 65 (6): 494–506. https://doi.org/10.1680/geot.14.P.192.
Zheng, J., R. D. Hryciw, and A. Ventola. 2017. "Compressibility of sands of various geologic origins at pre-crushing stress levels." *Geotech. Geol. Eng.* 35 (5): 2037–2051. https://doi.org/10.1007/s10706-017-0225-9.